J. Fluid Mech. (2013), *vol.* 716, *pp.* 566–596. © Cambridge University Press 2013
doi:10.1017/jfm.2012.557

A submerged cylinder wave energy converter

S. Crowley†, R. Porter and D. V. Evans

School of Mathematics, University of Bristol, Bristol BS8 1TW, UK

(Received 20 September 2012; revised 5 November 2012; accepted 6 November 2012)

A novel design concept for a wave energy converter (WEC) is presented and analysed. Its purpose is to balance the theoretical capacity for power absorption against engineering design issues which plague many existing WEC concepts. The WEC comprises a fully submerged buoyant circular cylinder tethered to the sea bed by a simple mooring system which permits coupled surge and roll motions of the cylinder. Inside the cylinder a mechanical system of pendulums rotate with power generated by the relative rotation rates of the pendulums and the cylinder. The attractive features of this design include: making use of the mooring system as a passive component of the power take off (PTO); using a submerged device to protect it from excessive forces associated with extreme wave conditions; locating the PTO within the device and using a PTO mechanism which does not need to be constrained; exploiting multiple resonances of the system to provide a broad-banded response. A mathematical model is developed which couples the hydrodynamic waves forces on the device with the internal pendulums under a linearized framework. For a cylinder spanning a wave tank (equivalent to a two-dimensional assumption) maximum theoretical power for this WEC device is limited to 50 % maximum efficiency. However, numerical results show that a systematically optimized system can generate theoretical efficiencies of more than 45 % over a 6 s range of wave period containing most of the energy in a typical energy spectrum. Furthermore, three-dimensional results for a cylinder of finite length provide evidence that a cylinder device twice the length of its diameter can produce more than its own length in the power of an equivalent incident wave crest.

Key words: surface gravity waves, wave scattering, wave–structure interactions

1. Introduction

The earliest recorded patent on a wave energy device was taken out by the Girard father and son in Paris in 1794. It was not until the mid-1970s when the price of oil quadrupled that the feasibility of extracting useful electrical energy from ocean waves was again considered seriously. In the UK this was stimulated by a key paper published in *Nature* by Salter (1974) in which he showed experimentally that a cam-shaped cylindrical section spanning a narrow wave tank was capable of absorbing over 80 % of the energy in the waves incident upon it. The potentially high efficiency of the Salter 'duck' prompted the UK government to initiate a major wave energy R&D programme aimed at estimating the cost of this renewable energy

† Email address for correspondence: sarah.crowley@bristol.ac.uk

https://doi.org/10.1017/jfm.2012.557 Published online by Cambridge University Press

if used on a large-scale to supply UK electricity needs. This was quickly followed by smaller programmes in Japan, Scandinavia, Portugal and the USA. These programmes attracted a wide range of scientists, engineers, theoreticians and industrialists and a large number of ideas for capturing wave energy were proposed, many of which were tested at varying scales in wave tanks or in a few cases in sea conditions at one-tenth scale. During this time the main theoretical principles underpinning ocean wave power absorption were established by extending ideas from ocean engineering and ship hydrodynamics. A contemporary review of the theory at that time can be found in Evans (1981). In 1982 the UK Department of Energy concluded that the overall economic prospects for wave energy looked poor when compared with other electricity-producing renewable energy technologies and the programme was terminated apart from some small-scale generic research, although research continued at a lower level outside the UK.

In the last decade or so concerns about the effect of global warming have prompted governments to revisit the potential for ocean wave power as an economically viable source of renewable energy and to encourage and support private industry in the development of new wave energy converters (WECs). In contrast to the 1970s, with one or two notable exceptions, as the sector moves towards commercial-scale prototypes, practical issues have dominated thinking. This is possibly because much of the mathematical framework is believed to be in place, but more likely from the recognition that the reliable and robust conversion of ocean wave power to electrical power is predominantly an engineering challenge involving considerations such as survivability and ease of engineering design in the harsh environment of the ocean surface. Examples of modern perspectives on wave power are given by Falnes (2007) and Cruz (2008).

In this paper we introduce a WEC which we believe addresses many of these overriding concerns while at the same time providing a firm mathematical basis for optimizing the power absorption of the device. The WEC can be thought of as a modification of the Bristol Cylinder device invented by one of the present authors and described in Evans *et al.* (1979) and Clare, Evans & Shaw (1982). The present version shares the advantages of the Bristol Cylinder in operating just below the ocean surface thereby shedding excessive power levels, and of moving in response to the incident waves in such a way as to reduce excessive wave loading and avoiding 'end stop' problems. In contrast to its predecessor it also has an internal power take off (PTO) system protected from the ocean which can be adjusted to optimize the energy extracted. The mooring of the cylinder is used as a passive component in the PTO system, allowing the cylinder to pitch about an axis parallel to that of the cylinder. Thus, the present device could also be regarded as being loosely related to number of nearshore and onshore devices operating in pitch–surge motions, the 'Oyster' device being the most well known of these in which a buoyant flap is hinged about its base and power is extracted from the pitching motion relative to the sea bed (see Folley, Whittaker & VantHoff 2007). Not everything about the new concept is an improvement on the old Bristol Cylinder idea. The main, significant, drawback follows from the fact that the Bristol Cylinder was shown theoretically, in two-dimensional motion, to be 100 % efficient (that is, all incoming wave energy is absorbed) at a particular tuned wave period. The current design, constrained to move in one degree of freedom as opposed to two, is at most 50 % efficient. The focus here then is to design a system which is effective over a wide range of wave periods.

Theory, and indeed physical intuition, dictates that a good wave energy absorber should be resonant and many WECs are designed with this in mind. Recently, Evans

https://doi.org/10.1017/jfm.2012.557 Published online by Cambridge University Press

& Porter (2012) described a number of theoretical devices which exhibit either coupled resonances or multiple resonances. The idea behind such concepts, which is again not new, is to tune devices to be resonant at more than one wave period so that the WEC is able to operate effectively over a wider range of periods with the realization that a real sea state is broad-banded and peak wave periods vary significantly over an annual cycle. The current idea of having multiple internal pendulums located within the device, tunable to different periods and each capable of taking off power is a natural development of these thoughts.

The use of relative motion of a mass moving internally within a buoyant structure to extract power from the ocean is not new. Thus, Parks (1980) investigates a range of simple WECs with internal, self-contained, resonant systems for power extraction. Advantage is taken of the tunability of such devices so that efficiency and bandwidth are optimal at a desired frequency. Likewise, Salter (1982) discusses the advantages of the use of gyros over a simpler pump mechanism to provide a frame of reference about which multiple 'ducks' on a spine may react in order to extract power. Korde (1990) proposes a smaller-scale application of wave energy conversion whereby the energy of a cylinder rolling on a circular track within a barge, which itself rolls in the sea waves, is extracted and used to generate a laser beam.

More recently, the floating SEAREV device has been developed (see Babarit *et al.* 2006, for example), which also has an internal component that behaves mechanically like a pendulum. Power is taken off through the relative motion between the floating body and the inner pendulum. The authors list two advantages of such a system, namely that all components relating to PTO are internal and thus protected from the sea environment and, second, due to the wheel shape of the inner pendulum there are no 'end-stop' problems (that is, the motion does not need to be limited or constrained as with many device concepts). Similarly Kashiwagi, Nishimatsu & Sakai (2012) introduce a floating device of square cross-section with another rotating pendulum-type PTO mechanism. It comprises two circular cylinders nested within one another, the smaller cylinder being allowed to rotate, without sliding, along the inner surface of the cylinder with the larger radius. The authors investigate the conditions required to maximize the device efficiency over a wide range of wave frequencies and find evidence of increased efficiency close to the resonant frequencies of both the floating body and the inner cylinder.

The detailed configuration of the device presented here is explained in § 3. However, before this, in § 2 we take a step back and consider a much simpler theoretical device concept. Here, we simply consider the cylinder pitching about a fixed point held under tension to the sea bed by the buoyancy of the cylinder. The purpose of this is twofold. First, we show that certain properties of a circular cylinder, related to its variation of added mass with frequency, mean that multiple resonances and, consequently, a broad-banded response can be achieved. This is based on the adoption of a PTO system which is unlikely to be successful in practice although similar PTOs have been previously suggested (see Chaplin & Aggidis 2007). Second, it allows the basic results, formulation and ideas needed for later sections to be introduced.

In § 3 the particular configuration of the device is described and the equations of motion for a general system of N internal pendulums rotating independently within the cylinder is described. Also, a general mooring system is used and parametrized by a number δ which governs how the roll of the cylinder is coupled to its pitch. Despite this generality, many of the results focus on $N = 1$ and $\delta = 1$. Two different approaches are given to the calculation of power, one limited to $N = 1$ pendulums, but capable of predicting the efficiency envelope or optimal power and the other method

https://doi.org/10.1017/jfm.2012.557 Published online by Cambridge University Press

not able to do this, but applicable to any number of pendulums. In § 4, results are presented first for a two-dimensional cylinder with internal pendulums focusing on how to determine the optimal configuration for a broad-banded response. Again it is shown that the best configuration exhibits multiple resonances (a cylinder with one internal pendulum can be resonant at five different wave periods) and leads to a broad-banded response. Optimization of 'full-scale' and 'half-scale' cylinder configurations are given. Later in § 4, results for a three-dimensional cylinder are presented. A short and long cylinder with internal pendulum PTO are optimized over a range of wave periods and the optimization is performed again, weighted by a model sea state showing that capture factors in excess of one are predicted.

2. A submerged pitching cylinder device

2.1. *Equation of motion*

This WEC device consists of a submerged buoyant circular cylinder with closed ends having radius a, length D and total mass M. The cylinder is held a distance f $(>a)$ below the surface and is constrained to pitch about a point, P, a distance, L, below the axis of the cylinder, O. In motion the line OP makes a clockwise angle Θ with respect to the vertical, see figure 1. The surrounding water, of density ρ, is of constant depth h which need not be equal to $L+f$.

Assuming small-amplitude motions, $\Theta \ll 1$, the vertical forces acting along the line OP balance the buoyancy forces acting on the cylinder given by $(M_w - M)g$ where M_w is the mass of water displaced by the cylinder. The horizontal component of force along OP due to the buoyancy is $(M_w - M)gL\sin\Theta \approx (M_w - M)gL\Theta$. Thus, Newton's Law applied to small-amplitude pitching motions about P gives

$$M(L^2 + K^2)\ddot{\Theta} = LF_w - (M_w - M)gL\Theta - \lambda L^2\dot{\Theta}, \tag{2.1}$$

where MK^2 is the moment of inertia of the cylinder about its axis O, F_w is the horizontal wave force in surge acting through O and the last term denotes an external linear damping force proportional to the rate of rotation of the cylinder about P, controlled by the damping constant λ.

Assuming incident waves of a single angular frequency ω, the surge force may be written $F_w = \mathrm{Re}\{X_w e^{-i\omega t}\}$ where X_w is a function of ω, whilst we write $L\dot{\Theta} = \mathrm{Re}\{Ue^{-i\omega t}\}$ so that U represents the complex horizontal velocity of the axis of the cylinder, O. Then (2.1) can be written

$$-i\omega M(1 + \hat{K}^2)U = X_w - \frac{i}{\omega}C_0 U + X_e, \tag{2.2}$$

where we introduced the dimensionless quantity $\hat{K} = K/L$, and defined

$$C_0 = \frac{g}{L}(M_w - M), \tag{2.3}$$

whilst

$$X_e = -\lambda U. \tag{2.4}$$

2.2. *Power calculation*

Standard theories of wave energy absorption can be applied to (2.2); see, for example, Cruz (2008, Ch. 3) or Evans & Porter (2012). Hence, the surge wave force on the cylinder can be decomposed using linearity into forces due to diffraction of a

https://doi.org/10.1017/jfm.2012.557 Published online by Cambridge University Press

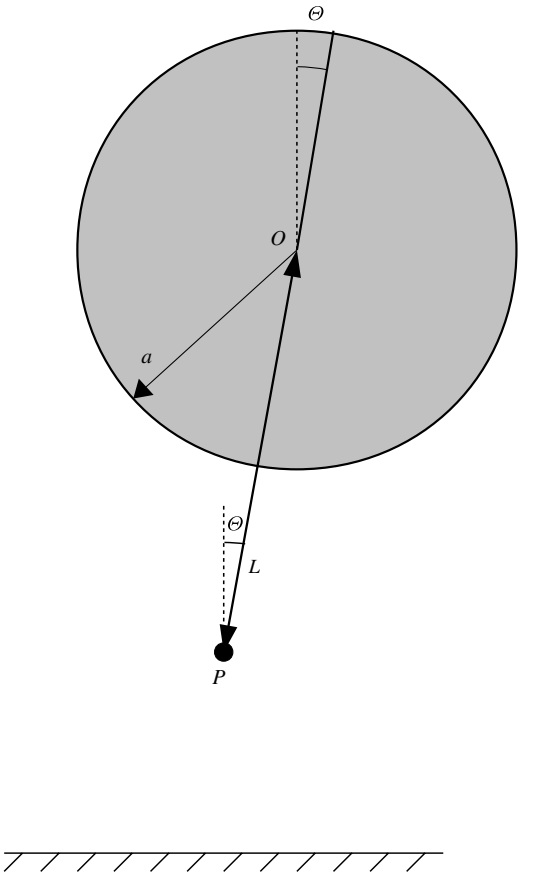


FIGURE 1. Definition of dimensions for the simple submerged buoyant circular cylinder WEC.

motionless cylinder, X_s, and those due to radiation, proportional to the velocity of the cylinder, X_r, that is

$$X_w = X_r + X_s \quad \text{with } X_r = (\mathrm{i}\omega A - B)U, \tag{2.5}$$

where X_r is represented in terms of the surge-induced added mass, $A(\omega)$, and radiation damping, $B(\omega)$, components both dependent on frequency.

Upon combining (2.2) and (2.4) with (2.5) one finds

$$(Z + \lambda)U = X_s, \tag{2.6}$$

where

$$Z \equiv B - \mathrm{i}\omega(A + M(1 + \hat{K}^2) - C_0/\omega^2). \tag{2.7}$$

The mean power (time averaged over a period) generated by the device is given by

$$W = \tfrac{1}{2}\mathrm{Re}\{X_w \overline{U}\}, \tag{2.8}$$

the overbar denoting conjugation of complex quantities. It follows from using (2.2) in (2.8) that

$$W = -\tfrac{1}{2}\mathrm{Re}\{X_e \overline{U}\} = \tfrac{1}{4}(\lambda + \overline{\lambda})\,|U|^2, \tag{2.9}$$

https://doi.org/10.1017/jfm.2012.557 Published online by Cambridge University Press

after using (2.4) where, for now, we have assumed λ to be complex. Using (2.6) to eliminate U and the identity

$$\frac{(\lambda+\overline{\lambda})}{|\lambda+Z|^2}=\frac{1}{2\mathrm{Re}\{Z\}}\left(1-\frac{|Z-\overline{\lambda}|^2}{|Z+\lambda|^2}\right), \tag{2.10}$$

the mean power is given by

$$W=\frac{|X_s|^2}{8B}\left(1-\frac{|\lambda-\overline{Z}|^2}{|\lambda+Z|^2}\right) \tag{2.11}$$

noting that $\mathrm{Re}\{Z\}=B$. It is well known that, in two dimensions, the quantities X_s and B are connected by the formula (see, for example, Newman 1976)

$$W_{inc}=\frac{|X_s|^2}{8B\eta}, \tag{2.12}$$

where W_{inc} is the mean power in an incident wave per unit length of wave crest. The term η is related to the wave-making ability of the device, via $\eta=|A_+|^2/(|A_-|^2+|A_+|^2)$ in terms of the radiated wave amplitudes $A_\pm$ towards $\pm\infty$ due to the forced motion of the device in surge motion in the absence of incident waves which would otherwise have arrived from $-\infty$. Here the circular cylinder moving in surge has fore–aft symmetry dictating that $|A_+|=|A_-|$ and implying that $\eta=1/2$.

Thus, in two dimensions, a WEC device may be characterized by the efficiency, the ratio of the power absorbed per length of the device to the power per length of wave crest in the incident wave,

$$E=\frac{W}{W_{inc}}=\eta\left(1-\frac{|\lambda-\overline{Z}|^2}{|\lambda+Z|^2}\right), \tag{2.13}$$

with a maximum of $E_{max}=\eta=1/2$ when $\lambda=\overline{Z}$, a result first obtained independently by Evans (1976), Mei (1976) and Newman (1976). The symmetry of the WEC device we are considering limits the efficiency in two dimensions to 1/2 or 50 % of the total available incident wave energy.

If, as envisaged from a practical perspective, λ is real, achieving maximum efficiency requires both

$$\lambda=B(\omega)\quad\text{and}\quad I(\omega)\equiv A(\omega)+M(1+\hat{K}^2)-C_0/\omega^2=0, \tag{2.14}$$

to be satisfied at the same frequency. It helps to derive alternative versions of (2.10) and (2.11) which apply to real-valued λ. Thus, instead of (2.10) we introduce the relation

$$\frac{2\lambda}{|\lambda+Z|^2}=\frac{1}{(|Z|+\mathrm{Re}\{Z\})}\left(1-\frac{(\lambda-|Z|)^2}{|\lambda+Z|^2}\right), \tag{2.15}$$

from which it follows that the efficiency can be expressed by

$$E=\eta\frac{2B}{(|Z|+B)}\left(1-\frac{(\lambda-|Z|)^2}{|\lambda+Z|^2}\right). \tag{2.16}$$

Again we note that $E=E_{max}$ if $\lambda=|Z|$ and $|Z|=B$ (in other words the conditions in (2.14)) hold. However (2.16) gives us an upper bound on the power available from

https://doi.org/10.1017/jfm.2012.557 Published online by Cambridge University Press

the WEC when λ is constrained to be real given by

$$E_{opt} = \eta \frac{2B}{(|Z| + B)} = \frac{B}{(|Z| + B)}. \tag{2.17}$$

2.3. *Results and discussion*

The success of this concept (and any WEC device that has no control over the imaginary part of a complex damping parameter, λ) requires that the inertia term

$$|I(\omega)| \ll B(\omega)/\omega \tag{2.18}$$

over a wide range of frequencies, since then E_{opt} will be close to E_{max} over that range. Values of ω such that $I(\omega) = 0$ are identifiable as resonances of the system and, whilst $A(\omega)$ is evidently dependent on frequency, it is clear to see that such a resonance should exist. Since the hydrostatic 'spring' term, C_0, is positive for the cylinder to be buoyant and $A(\omega)$ tends to positive constants denoted by $A(0)$ and $A(\infty)$ as $\omega \to 0$ and $\omega \to \infty$, we readily confirm that

$$I(\omega) \to -\infty \text{ as } \omega \to 0 \text{ whilst } I(\omega) \to A(\infty) + M(1 + \hat{K}^2) > 0 \quad \text{as } \omega \to \infty. \tag{2.19}$$

Since $A(\omega)$ is non-singular, there is at least one value of ω satisfying $I(\omega) = 0$. This is, of course, unsurprising: a submerged buoyant cylinder rotating about a fixed point below its axis acts as an upturned pendulum and so we expect it to exhibit resonance. What is perhaps more surprising is that it is possible to configure a submerged pitching cylinder which possesses multiple resonances. The key lies in the variation of the added mass with ω for the circular cylinder which can be shown behaves roughly like $\alpha + \beta/\omega^2$ (where α and β are constants) over a range of values of ω for cylinders close enough to the surface. Thus, it is possible to find arrangements in which $I(\omega)$ is close to zero over a broad range of values of ω and, in fact, passes through zero for three values of ω.

These features are illustrated in figure 2(*a*) where the dimensionless added mass coefficient $\mu = A(\omega)/M_w$ is plotted against the period $T = 2\pi/\omega$ (in seconds) of motion for three submergence ratios, $a/f = 0.6$, 0.75 (highlighted) and 0.9. For these results, we have used $h = 50$ m and $a = 7$ m, $K^2 = 0.8a^2$ and $M/M_w = 0.15$. Plotted on the same graph is the dimensionless quantity $(A(\omega) - I(\omega))/M_w$ for three different dimensionless mooring lengths, $L/a = 1/2$, 1 and 2.

Each one of these three latter curves is exactly quadratic on these axes whilst the curves of added mass are roughly quadratic over periods between 6 and 10 s. Note that curves of $(A(\omega) - I(\omega))/M_w$ depend upon the mooring length, L/a, but not the submergence, a/f, whilst the opposite is true for curves of $A(\omega)/M_w$. Thus, intersections between any of the three chained lines of $(A(\omega) - I(\omega))/M_w$ and any of the $A(\omega)/M_w$ curves are points where $I(\omega) = 0$; in other words resonances.

Most pairs of curves intersect just once. However, note that the pair of curves $a/f = 0.9$ and $L/a = 2$ intersect at three points indicating three distinct resonances at periods close to 12.5, 8 and 4.5 s. Also note that the pair of curves labelled $a/f = 0.75$ and $L/a = 2$ remain close together, implying $I(\omega)$ is close to zero, over a range of periods from 6 to 11 s. As indicated above, this feature will result in the potential for a broad-banded response in the WEC efficiency as demonstrated by curves in figure 2(*b*) for the optimum efficiency for a real damping coefficient, E_{opt}, against period. Here we have fixed submergence $a/f = 0.75$ but vary L/a. Hence, for $L/a = 2$, the optimum efficiency curve remains close to the maximum of a half over periods from 6 to 11 s. In contrast, smaller values of L/a where $I(\omega) = 0$ just once and the

https://doi.org/10.1017/jfm.2012.557 Published online by Cambridge University Press

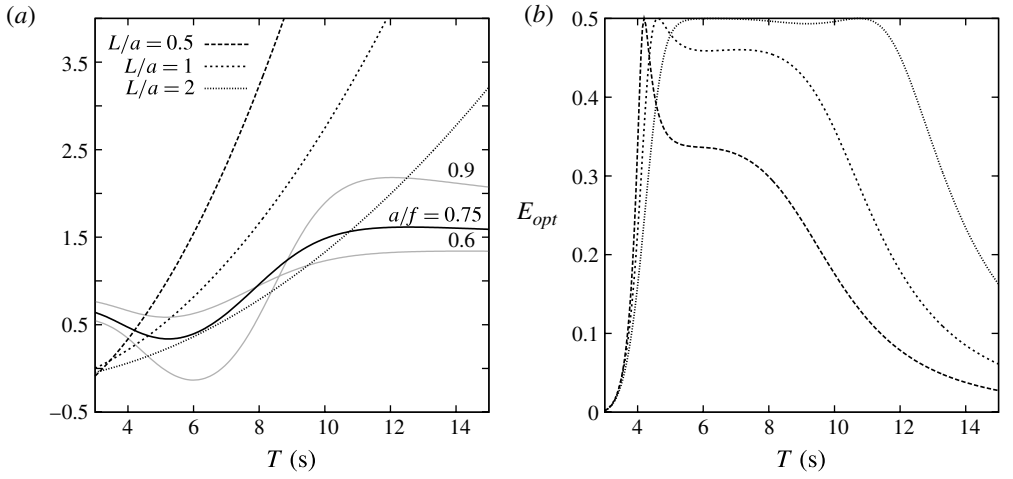


FIGURE 2. A pitching cylinder WEC device: $h = 50$ m, $a = 7$ m, $M/M_w = 0.15$. In (a) $(A(\omega) - I(\omega))/M_w$ is plotted for $L/a = 1/2$, 1 and 2 (chained curves) and $A(\omega)/M_w$ is plotted for $a/f = 0.6$, 0.75 and 0.9. In (b) the corresponding upper bound of efficiency E_{opt} is shown for fixed $a/f = 0.75$ and $L/a = 1/2$, 1 and 2.

divergence of the pairs of curves $a/f = 0.75$ and $L/a = 1, 1/2$ in figure 2(a) is more pronounced lead to much narrower peaks to maximum values in E_{opt}.

3. A cylinder with internal pendulums

3.1. *Description of the device*

In the previous section we have demonstrated the potential of a submerged pitching cylinder WEC which exploits multiple resonances under certain configurations to produce a broad-banded efficiency over a range of physically relevant wave periods. However, for such a device, power is designed to be generated from the rotation of the device with respect to the fixed pivot about which the cylinder is constrained to pitch. The principal purpose of this pivot is to hold the cylinder under tension below the surface. It is difficult to envisage a robust practical engineering solution to cope with the additional forces required by a PTO mechanism attached through the pivot.

It is widely recognized amongst wave energy specialists that PTOs contained internally within a device are the most desirable from an engineering design perspective, see for example Falcão (2010) with reference to the SEAREV and Frog devices. Thus, we take the submerged cylinder idea of the previous sections forward by allowing the submerged buoyant cylinder to pitch freely about the pivot and instead place the PTO inside the cylinder by means of an internal pendulum system which we continue to describe in detail below.

For generality, assume a hollow cylinder contains N compound pendulums each designed to rotate about the cylinder axis. All pendulums are assumed to have the same density, ρ_s, and each pendulum has a uniform cross-section and spans an equal proportion, D/N, of the total cylinder length.

The specific pendulum design considered here is composed of an annular cross-section, with a common outer radius a to coincide with the cylinder radius, an inner radius $b_i < a$, $i = 1, \ldots, N$, and subtends an angle of $2\alpha_i$ (see figure 3). Thus, the ith pendulum has mass $m_i = \rho_s \alpha_i (a^2 - b_i^2) D/N$ and is pivoted about the axis of the cylinder.

https://doi.org/10.1017/jfm.2012.557 Published online by Cambridge University Press

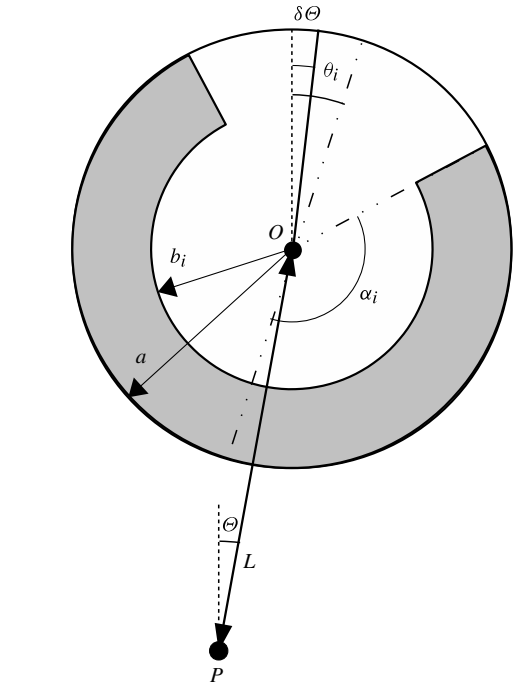


FIGURE 3. Definition of dimensions for the WEC and pendulum system.

These masses do not contribute towards the mass, M, of the cylinder which we have defined previously. A linear damping mechanism is connected to each pendulums, which acts in proportion to the rate of rotation of the pendulums with respect to that of the cylinder.

Each compound pendulum has its own natural length, l_i, being the distance of the centre of mass to its pivot defined by

$$l_i = \frac{2a \sin \alpha_i}{3\alpha_i} \frac{(1 + \hat{b}_i + \hat{b}_i^2)}{1 + \hat{b}_i}, \tag{3.1}$$

where $\hat{b}_i = b_i/a$. Each pendulum also has a moment of inertia about its centre of mass, $m_i k_i^2$, where k_i is the radius of gyration of the ith pendulum, and this is given by

$$k_i^2 = \tfrac{1}{2}a^2(1 + \hat{b}_i^2) - l_i^2. \tag{3.2}$$

Finally, each pendulum has, in the absence of damping, a resonant period given, for small amplitudes, by

$$T_i = \frac{2\pi}{\omega_i} \quad \text{with } \omega_i^2 = \frac{g}{l_i + k_i^2/l_i}. \tag{3.3}$$

https://doi.org/10.1017/jfm.2012.557 Published online by Cambridge University Press

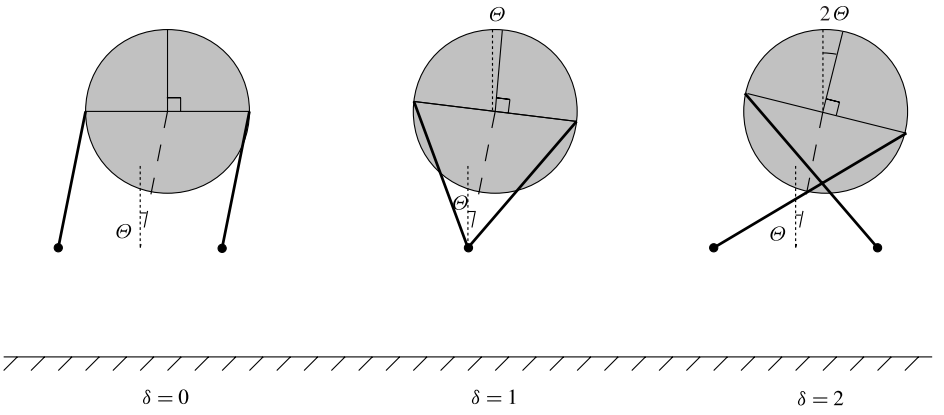


FIGURE 4. Various tether configurations.

Then as $\alpha_i \to 0$, and $\hat{b}_i \to 1$ we recover a point mass pendulum in which $l_i \to a$ and $k_i \to 0$ and $T_i = 2\pi\sqrt{a/g}$. When $\alpha_i \to \pi$, $l_i \to 0$ and the period approaches infinity. The attraction of this system is that each internal compound pendulum can be tuned to its own resonant period within the range of physically relevant periods.

Having separated the PTO mechanism, through the use of internal pendulums, from the mooring system we are able to consider a more general design in the way in which the device is constrained to pitch about its pivot point P. An example of an alternative mooring system is one in which tethers are designed to induce varying degrees of roll of the cylinder about its axis, O, in proportion, δ, to the angular displacement of the cylinder about the point P. Three such mooring systems are represented in figure 4 in which the cylinder rotates through an angle $\delta\Theta$ with $\delta = 0$, 1 and 2. These integer values of δ are examples of a continuous range of cylinder rotation rates determined by the attachments of the mooring lines. The value $\delta = 1$ corresponds to the mooring system used in § 2 and is the easiest to implement practically.

3.2. *Equations of motion*

The added complication of a system of internal compound pendulums means that equations of motion are most easily derived from the Euler–Lagrange equations. Generalized coordinates Θ and θ_i, for $i = 1, \ldots, N$, are used to represent the angle of roll of the cylinder and those of the pendulums with respect to the vertical (see figure 3). Thus, the potential energy for the system is given by

$$\mathscr{V}(\Theta, \theta_1, \ldots, \theta_N) = -(M_w - M)gL\cos\Theta + \sum_{i=1}^{N} m_i g(L\cos\Theta - l_i\cos\theta_i), \qquad (3.4)$$

where M_w is the mass of water displaced by the cylinder as before and M is the mass of the cylinder not including internal pendulums.

The kinetic energy for the system is given by

$$\mathscr{T}(\Theta, \theta_1, \ldots, \theta_N) = \frac{1}{2}ML^2\dot{\Theta}^2 + \frac{1}{2}M\delta^2K^2\dot{\Theta}^2 + \frac{1}{2}\sum_{i=1}^{N} m_i k_i^2\dot{\theta}_i^2$$
$$+ \frac{1}{2}\sum_{i=1}^{N} m_i\left(L^2\dot{\Theta}^2 + l_i^2\dot{\theta}_i^2 - 2Ll_i\dot{\Theta}\dot{\theta}_i\cos(\Theta - \theta_i)\right). \qquad (3.5)$$

https://doi.org/10.1017/jfm.2012.557 Published online by Cambridge University Press

The linearized damping is included via the Rayleigh dissipation function (see Goldstein 1974), with

$$\mathscr{D}(\Theta, \theta_1, \ldots, \theta_N) = \frac{1}{2}\sum_{i=1}^{N} \gamma_i l_i^2 \left(\dot{\theta}_i - \delta\dot{\Theta}\right)^2, \tag{3.6}$$

where γ_i is the damping coefficient proportional to the differential rate of rotation of the pendulums and the cylinder.

The Euler–Lagrange equations are given by

$$\frac{\partial}{\partial t}\frac{\partial \mathscr{L}}{\partial \dot{\Theta}} - \frac{\partial \mathscr{L}}{\partial \Theta} + \frac{\partial \mathscr{D}}{\partial \dot{\Theta}} = LF_w \tag{3.7}$$

$$\frac{\partial}{\partial t}\frac{\partial \mathscr{L}}{\partial \dot{\theta}_i} - \frac{\partial \mathscr{L}}{\partial \theta_i} + \frac{\partial \mathscr{D}}{\partial \dot{\theta}_i} = 0 \quad \text{for } i = 1, \ldots, N, \tag{3.8}$$

where $\mathscr{L} = \mathscr{T} - \mathscr{V}$ and F_w represents the external horizontal wave force applied to the cylinder, as before.

Application of (3.7) and (3.8) followed by a linearization of the variables on the assumption that $|\Theta| \ll 1$ and $|\theta_i| \ll 1$ for all i leads to

$$M\left(L + \delta^2\frac{K^2}{L}\right)\ddot{\Theta} + \sum_{i=1}^{N} m_i(L\ddot{\Theta} - l_i\ddot{\theta}_i) = F_w - (M_w - M)g\Theta + \sum_{i=1}^{N} m_i g\Theta + \delta\sum_{i=1}^{N}\gamma_i\frac{l_i^2}{L}(\dot{\theta}_i - \delta\dot{\Theta}), \tag{3.9}$$

and

$$m_i\frac{k_i^2}{l_i}\ddot{\theta}_i + m_i(l_i\ddot{\theta}_i - L\ddot{\Theta}) = -m_i g\theta_i - \gamma_i l_i(\dot{\theta}_i - \delta\dot{\Theta}) \quad \text{for } i = 1, \ldots, N, \tag{3.10}$$

where these equations have been re-ordered into a form suggestive of Newton's law.

We consider the single-frequency response of the device to single-frequency wave forcing, as in § 2 and re-use notation introduced there. Here, we have an additional dynamic variable $\dot{\theta}_i$ replaced by a time-harmonic factorized equivalent using $l_i\dot{\theta}_i = \mathrm{Re}\{u_i \mathrm{e}^{-\mathrm{i}\omega t}\}$, so that u_i is now frequency dependent and represents the complex horizontal velocity of the pendulum's centre of mass with respect to the cylinder centre.

Then the two equations of motion, (3.9) and (3.10), may be written as

$$-\mathrm{i}\omega M(1 + \delta^2\hat{K}^2)U - \mathrm{i}\omega\sum_{i=1}^{N} m_i(U - u_i) = X_w - \frac{\mathrm{i}}{\omega}C_N U + \delta\sum_{i=1}^{N}\hat{l}_i\gamma_i(u_i - \delta\hat{l}_i U) \tag{3.11}$$

and

$$-\mathrm{i}\omega m_i\hat{k}_i^2 u_i - \mathrm{i}\omega m_i(u_i - U) = -\frac{\mathrm{i}}{\omega}c_i u_i - \gamma_i(u_i - \delta\hat{l}_i U), \tag{3.12}$$

respectively, where we have developed earlier shorthand notation by defining

$$C_N = \left(M_w - M - \sum_{i=1}^{N} m_i\right)\frac{g}{L} \quad \text{and} \quad c_i = \frac{m_i g}{l_i}. \tag{3.13}$$

https://doi.org/10.1017/jfm.2012.557 Published online by Cambridge University Press

(the former required to be positive for the cylinder to be buoyant) and dimensionless quantities

$$\hat{l}_i = \frac{l_i}{L}, \quad \hat{k}_i = \frac{k_i}{l_i}. \tag{3.14}$$

Equations (3.11) and (3.12) represent $N+1$ equations for the $N+1$ unknowns U and u_i, $i = 1, \ldots, N$, noting that the system is forced comes from one of the components of X_w, the other component being proportional to U (see (2.5)).

There are two ways in which one may proceed each with its own merits. First, since each u_i is connected only to U (rather than the other u_is) as demonstrated in (3.12), it is possible to eliminate the u_is from (3.11) in favour of a single equation for U, expressed in the form of (2.2) and (2.4). At this point the standard results of § 3 for power calculations can be used.

A second approach seems more immediately obvious, which is to assemble (3.11) and (3.12) into a single matrix analogue of (2.2). As we shall see later, some care is needed over the structure of these equations and, related to this, how to develop appropriate power calculations.

3.3. *First method*

The process of deriving equations of motion from resolving forces leads more naturally to a revised form of (3.11) in which the second acceleration term is substituted from (3.12) to give

$$-\mathrm{i}\omega M(1+\delta^2\hat{K}^2)U - \mathrm{i}\omega\sum_{i=1}^{N} m_i\hat{k}_i^2 u_i = X_w - \frac{\mathrm{i}}{\omega}C_N U - \frac{\mathrm{i}}{\omega}\sum_{i=1}^{N} c_i u_i - \sum_{i=1}^{N}\gamma_i(1-\delta\hat{l}_i)(u_i - \delta\hat{l}_i U). \tag{3.15}$$

Then the equations of motion, (3.12) and (3.15), may be written as

$$-\mathrm{i}\omega M(1+\delta^2\hat{K}^2)U = X_w - \frac{\mathrm{i}}{\omega}C_N U + X_e, \tag{3.16}$$

and

$$(\hat{\Omega}_i + \mathrm{i}\hat{\gamma}_i)u_i = (1 + \mathrm{i}\hat{\gamma}_i\hat{l}_i\delta)U, \quad i = 1, \ldots, N, \tag{3.17}$$

respectively, whilst

$$X_e = -\sum_{i=1}^{N} m_i\omega\hat{\gamma}_i(1-\delta\hat{l}_i)(u_i - \delta\hat{l}_i U) - \frac{\mathrm{i}}{\omega}\sum_{i=1}^{N} c_i u_i + \mathrm{i}\omega\sum_{i=1}^{N} m_i\hat{k}_i^2 u_i. \tag{3.18}$$

It has helped the presentation to define non-dimensional variables

$$\hat{\Omega}_i = \frac{g}{l_i}\left(\frac{1}{\omega_i^2} - \frac{1}{\omega^2}\right) \quad \text{and} \quad \hat{\gamma}_i = \frac{\gamma_i}{m_i\omega}, \tag{3.19}$$

where ω_i is the resonant frequency of the ith pendulum, given by (3.3).

Using (3.17) in (3.18) gives

$$X_e = -\lambda U, \tag{3.20}$$

https://doi.org/10.1017/jfm.2012.557 Published online by Cambridge University Press

where, after some algebra, we find

$$\lambda = \sum_{i=1}^{N} \frac{\mathrm{i}m_i\omega}{\hat{\Omega}_i + \mathrm{i}\hat{\gamma}_i} \left((\hat{\Omega}_i + \mathrm{i}\hat{\gamma}_i)\,(1 + \mathrm{i}\hat{\gamma}_i\delta\hat{l}_i)^2 - (1 + \mathrm{i}\hat{\gamma}_i\delta^2\hat{l}_i^2) \right). \tag{3.21}$$

As envisaged, (3.16) with (3.20) are the analogues of (2.2) and (2.4) in § 2 although λ, instead of being a real damping coefficient, is now a complex quantity being a nonlinear combination of the real damping coefficients γ_i acting on each of the pendulums.

The equations of motion for the new cylinder device and internal pendulum arrangement described in this section connect in the same way as before to the external hydrodynamic problem through the velocity U of the cylinder and the horizontal wave force, X_w, on the cylinder (see (2.5)). In order to calculate the power absorbed by the device we follow the same calculations described in § 2.2, noting that λ is now complex. Thus, the mean power developed by this WEC is given by (2.11) as before but with λ replaced by (3.21) and (2.7) replaced by

$$Z = B - \mathrm{i}\omega(A + M(1 + \delta^2\hat{K}^2) - C_N/\omega^2). \tag{3.22}$$

We note, in passing, that at an intermediate stage of the calculation of mean power given by (2.9) we find $W = |U|^2\,\mathrm{Re}\{\lambda\}/2$. Then

$$\mathrm{Re}\{\lambda\} = \sum_{i=1}^{N} \frac{m_i\omega\hat{\gamma}_i}{|\hat{\Omega}_i + \mathrm{i}\hat{\gamma}_i|^2}\,(1 - \delta\hat{l}_i\hat{\Omega}_i)^2 \tag{3.23}$$

follows from (3.21) which demonstrates that power generated by the device is, as expected, non-negative.

An alternative power calculation is available, in which the mean power generated by the WEC is given by the sum of the mean power generated by each of the pendulums. This is given by the time-averaged rate of working of the couple forces due to damping on the relative angular velocity of the pendulums to that of the cylinder, or

$$W = \frac{1}{2}\mathrm{Re}\left\{ \sum_{i=1}^{N} \gamma_i\,|u_i - \delta\hat{l}_i U|^2 \right\}, \tag{3.24}$$

after conversion to linear velocities. With use of (3.17) we find

$$W = \frac{1}{2}\,|U|^2 \sum_{i=1}^{N} \frac{m_i\omega\hat{\gamma}_i}{|\hat{\Omega}_i + \mathrm{i}\hat{\gamma}_i|^2}\,(1 - \delta\hat{l}_i\hat{\Omega}_i)^2, \tag{3.25}$$

which coincides with the expression for mean power derived from (3.23) above.

As discussed previously, with the efficiency given by (2.13), the maximum efficiency of $E_{max} = 1/2$ for the device is obtained when $\lambda = \overline{Z}$ where λ and Z are given by (3.21) and (3.22). Owing to the particular dependence of the complex-valued λ upon the damping coefficients γ_i it is far from obvious if and when this maximum power condition may be met. In other words, unlike the simple pitching cylinder device described earlier in the paper, there is no obvious formula for prescribing γ_i to obtain optimal or maximum power, even in the case of $N = 1$ pendulum.

The second method helps in this respect although, as we shall see, its usefulness is restricted to only $N = 1$ pendulum.

https://doi.org/10.1017/jfm.2012.557 Published online by Cambridge University Press

3.4. *Second method*

The aim here is to develop a matrix analogue of (2.2) by formulating a system of equations for the cylinder and pendulum motion whose structure allows a subsequent power calculation to be most easily formulated. To this end, we first make the change of variables from u_i to v_i via

$$v_i = u_i - \delta \hat{l}_i U, \quad i = 1, \ldots, N \tag{3.26}$$

which is a more natural representation of the internal pendulum excursion, being related through v_i to the difference between pendulum and cylinder angular velocities.

Under this variable change (3.11) and (3.12) become

$$-\mathrm{i}\omega M(1+\delta^2\hat{K}^2)U - \mathrm{i}\omega \sum_{i=1}^{N} m_i \left((1-\delta\hat{l}_i)U - v_i\right) = X_w - \frac{\mathrm{i}}{\omega} CU + \delta \sum_{i=1}^{N} \hat{l}_i \gamma_i v_i \tag{3.27}$$

and

$$-\mathrm{i}\omega m_i \hat{k}_i^2 (v_i + \delta\hat{l}_i U) - \mathrm{i}\omega m_i \left(v_i - (1-\delta\hat{l}_i)U\right) = -\frac{\mathrm{i}}{\omega} c_i (v_i + \delta\hat{l}_i U) - \gamma_i v_i, \tag{3.28}$$

(for $i = 1, \ldots, N$), respectively.

We take (3.28) and multiply through by $\delta\hat{l}_i$, sum the resulting equations from $i = 1, \ldots, N$, and add the sum to (3.27). This process is designed to eliminate all terms relating to the damping from the first equation. The result is

$$-\mathrm{i}\omega M(1+\delta^2\hat{K}^2)U - \mathrm{i}\omega \sum_{i=1}^{N} m_i(1-\delta\hat{l}_i)U - \mathrm{i}\omega \sum_{i=1}^{N} m_i(\delta\hat{l}_i(1+\hat{k}_i^2) - 1)(v_i + \delta\hat{l}_i U)$$

$$= X_w - \frac{\mathrm{i}}{\omega} C'_N U - \frac{\mathrm{i}}{\omega} \sum_{i=1}^{N} c'_i v_i \tag{3.29}$$

where

$$C'_N = C_N + \sum_{i=1}^{N} c_i \delta^2 \hat{l}_i^2 \quad \text{and} \quad c'_i = c_i \delta \hat{l}_i \equiv \frac{m_i g}{L}\delta. \tag{3.30}$$

After some rearranging, (3.28) and (3.29) for $i = 1, \ldots, N$ can be written in matrix/vector form,

$$-\mathrm{i}\omega \boldsymbol{M}\boldsymbol{U} = \boldsymbol{X}_w - \frac{\mathrm{i}}{\omega}\boldsymbol{C}\boldsymbol{U} + \boldsymbol{X}_e, \tag{3.31}$$

where the vectors of length $N+1$ are given by

$$\boldsymbol{U} = (U, v_1, \ldots, v_N)^{\mathrm{T}}, \quad \boldsymbol{X}_w = (X_w, 0, \ldots, 0)^{\mathrm{T}} \quad \text{and} \quad \boldsymbol{X}_e = (0, -\gamma_1 v_1, \ldots, -\gamma_N v_N)^{\mathrm{T}} \tag{3.32}$$

The 'mass' matrix $\boldsymbol{M}$ is symmetric with elements

$$\boldsymbol{M}_{00} = M(1+\delta^2\hat{K}^2) + \sum_{i=1}^{N} m_i \left((1-\delta\hat{l}_i)^2 + (\delta\hat{l}_i\hat{k}_i)^2\right), \tag{3.33a}$$

$$\boldsymbol{M}_{0i} = \boldsymbol{M}_{i0} = -m_i(1 - \delta\hat{l}_i - \delta\hat{l}_i\hat{k}_i^2) \quad \text{for } i \geqslant 1 \tag{3.33b}$$

$$\boldsymbol{M}_{ij} = m_i(1+\hat{k}_i^2)\delta_{ij} \quad \text{for } i, j \geqslant 1 \tag{3.33c}$$

https://doi.org/10.1017/jfm.2012.557 Published online by Cambridge University Press

where δ_{ij} represent the Kronecker delta function, whilst the 'restoring force' matrix $\boldsymbol{C}$ is also symmetric, with elements

$$\boldsymbol{C}_{00} = C'_N, \quad \boldsymbol{C}_{0i} = \boldsymbol{C}_{i0} = c'_i \quad \text{and} \quad \boldsymbol{C}_{ij} = c_i\delta_{ij}, \tag{3.34}$$

for $i, j = 1, \ldots, N$.

We may regard (3.31) as the analogue of (2.2) although it not obvious how to interpret physically the various terms that arise in the matrix elements above.

However, under the definitions above, the total mean power absorbed by the device is now given simply by

$$W = \tfrac{1}{2}\mathrm{Re}\{\boldsymbol{X}_w^*\boldsymbol{U}\} = -\tfrac{1}{2}\mathrm{Re}\{\boldsymbol{X}_e^*\boldsymbol{U}\}, \tag{3.35}$$

where * denotes the complex conjugate transpose. The second equation arises from using (3.31) and the fact that $\boldsymbol{M}$ and $\boldsymbol{C}$ are real. The first of the two expressions in (3.35) measures the power taken by the cylinder (equivalent to (2.7)) and the second the power generated by the internal pendulums (equivalent to (3.24)).

General results for wave power absorption by systems with more than one degree of freedom are well known (see Evans 1980; Falnes 2002 for example). However, these general results require that complex damping parameters couple each independent mode of the system to another independent mode. In other words there is a requirement that the system contains an $(N + 1)$-square matrix of unconstrained complex damping coefficients. This is not the case in this internal pendulum design where power is taken off due to the N pendulums only (i.e. the pitching cylinder is passive in PTO terms) and their rotation relative to that of the cylinder, not to each other. In other words, we have envisaged a system in which power is generated by just N real damping coefficients, γ_i.

There is little in the way of theoretical results for optimizing PTO when power is taken off either in fewer modes than the device is allowed to operate under or when coupling between different modes is not constrained. Of note is the work of Evans (1980) of which a few details are given in Cruz (2008) although there are no results of obvious use in this case. We can, however, make progress when there is just one pendulum, as outlined below.

3.5. *Calculations for a device with one pendulum*

If $N = 1$ and there is only one pendulum in the device then the matrix/vector system in (3.31) is of degree two. However, since damping is only taken off from the single internal pendulum, we may factorize the damping coefficient γ_1 from the matrix/vector system by writing

$$\boldsymbol{X}_e = -\gamma_1\boldsymbol{G}\boldsymbol{U}, \tag{3.36}$$

where

$$\boldsymbol{G} = \begin{pmatrix} 0 & 0 \\ 0 & 1 \end{pmatrix}. \tag{3.37}$$

Now the structure of (3.36) appears more closely related to that of § 2 as opposed to that pursued in the first method with (3.20) and (3.21).

From (3.35) we have

$$W = \tfrac{1}{2}\gamma_1\boldsymbol{U}^*\boldsymbol{G}\boldsymbol{U}, \tag{3.38}$$

to provide an expression for the mean power absorbed by the device in terms of the damping coefficient γ_1, which is assumed real. All that is required is an

https://doi.org/10.1017/jfm.2012.557 Published online by Cambridge University Press

equation for $\boldsymbol{U}$ relating the velocity of the cylinder and internal pendulums to the external hydrodynamic problem such that it can be eliminated from (3.38). The scalar equation (2.5) can be recast in matrix form as

$$\boldsymbol{X}_w = (\mathrm{i}\omega\boldsymbol{A} - \boldsymbol{B})\boldsymbol{U} + \boldsymbol{X}_s, \tag{3.39}$$

where $\boldsymbol{X}_s = (X_s, 0, \ldots, 0)^{\mathrm{T}}$ and the added mass and radiation damping matrices $\boldsymbol{A}$ and $\boldsymbol{B}$ only contain non-zero entries in the top left-hand corners. That is, $\boldsymbol{A}_{ij} = A\delta_{i0}\delta_{j0}$ and $\boldsymbol{B}_{ij} = B\delta_{i0}\delta_{j0}$ where A and B are the scalar added mass and radiation damping coefficients defined earlier. Thus, using (3.31), (3.36) and (3.39) we have

$$\boldsymbol{X}_s = (\boldsymbol{Z} + \gamma_1\boldsymbol{G})\boldsymbol{U}, \tag{3.40}$$

where, now, we have a matrix version of (2.7) given by

$$\boldsymbol{Z} \equiv \boldsymbol{B} - \mathrm{i}\omega(\boldsymbol{A} + \boldsymbol{M} - \omega^{-2}\boldsymbol{C}). \tag{3.41}$$

With (3.38) and (3.40) written in this manner, the damping coefficient associated with the single internal pendulum is seen explicitly and the equations are in a form that may allow us to find a value of γ_1 with which to obtain maximum power.

Using (3.40) in (3.38) we write

$$W = \tfrac{1}{2}\gamma_1 \boldsymbol{X}_s^* \boldsymbol{E}^* \boldsymbol{G}\boldsymbol{E}\boldsymbol{X}_s, \tag{3.42}$$

where $\boldsymbol{E} = (\boldsymbol{Z} + \gamma_1\boldsymbol{G})^{-1}$, the components of which can be calculated explicitly. We continue by assuming that the elements of $\boldsymbol{Z}$ in (3.41) are assigned $\boldsymbol{Z}_{ij}$ for $i, j = 0, 1$ and recall that $\boldsymbol{G}$ is given by (3.37) such that

$$\boldsymbol{E} = \frac{1}{\Delta}\begin{pmatrix} \boldsymbol{Z}_{11} + \gamma_1 & -\boldsymbol{Z}_{01} \\ -\boldsymbol{Z}_{10} & \boldsymbol{Z}_{00} \end{pmatrix} \quad \text{where } \Delta = (\boldsymbol{Z}_{11} + \gamma_1)\boldsymbol{Z}_{00} - \boldsymbol{Z}_{01}^2, \tag{3.43}$$

and the fact that $\boldsymbol{Z}$ is symmetric has been used. It can be shown that

$$\boldsymbol{X}_s^* \boldsymbol{E}^* \boldsymbol{G}\boldsymbol{E}\boldsymbol{X}_s = \frac{|X_s|^2\,|\boldsymbol{Z}_{01}|^2}{|\Delta|^2}, \tag{3.44}$$

with which, after setting

$$Z_1 = \boldsymbol{Z}_{11} - \frac{\boldsymbol{Z}_{01}^2}{\boldsymbol{Z}_{00}} \quad \text{such that } \Delta = \boldsymbol{Z}_{00}(Z_1 + \gamma_1), \tag{3.45}$$

equation (3.42) becomes

$$W = \frac{|X_s|^2}{2}\frac{\gamma_1\,|\boldsymbol{Z}_{01}|^2}{|\gamma_1 + Z_1|^2\,|\boldsymbol{Z}_{00}|^2}. \tag{3.46}$$

Since γ_1 is taken to be real we reuse the identity (2.15), with Z_1 replacing Z, such that the power may be written

$$W = \frac{|X_s|^2}{4}\frac{|\boldsymbol{Z}_{01}|^2 / |\boldsymbol{Z}_{00}|^2}{(|Z_1| + \mathrm{Re}\{Z_1\})}\left(1 - \frac{(\gamma_1 - |Z_1|)^2}{|\gamma_1 + Z_1|^2}\right). \tag{3.47}$$

The efficiency is W/W_{inc} with W_{inc} defined by (2.12) and noting that $\mathrm{Re}\{Z_1\} = B\,|\boldsymbol{Z}_{01}/\boldsymbol{Z}_{00}|^2$ this gives

$$E = \eta\frac{2B}{(B + |\boldsymbol{Z}_{00}/\boldsymbol{Z}_{01}|^2\,|Z_1|)}\left(1 - \frac{(\gamma_1 - |Z_1|)^2}{|\gamma_1 + Z_1\,|^2}\right), \tag{3.48}$$

https://doi.org/10.1017/jfm.2012.557 Published online by Cambridge University Press

from which the maximum achievable efficiency may be written

$$E_{opt} = \eta \frac{2B}{(B + |\boldsymbol{Z}_{00}||1 - \boldsymbol{Z}_{11}\boldsymbol{Z}_{00}/\boldsymbol{Z}_{01}^2|)}, \tag{3.49}$$

which is obtained when $\gamma_1 = |Z_1|$. Furthermore, if this is satisfied when $\mathrm{Im}\{Z_1\} = 0$, such that $|Z_1| = \mathrm{Re}\{Z_1\}$, then $E_{opt} = E_{max} = \eta$.

Thus, for $N = 1$ pendulum we have derived conditions needed to obtain maximum power: that $\mathrm{Im}\{Z_1\} = 0$ and that $\gamma_1 = \mathrm{Re}\{Z_1\} = B\,|\boldsymbol{Z}_{01}/\boldsymbol{Z}_{00}|^2$. Moreover, we have developed an expression for the 'envelope' of maximum power E_{opt} which assumes that γ_1 is tuned optimally as a function of frequency. Both of these features are obscured in the first method in this section. However, this second method has a restricted practical use to just one internal pendulum whereas the first method can be used for any number of pendulums.

As with the submerged pitching cylinder with no internal pendulums, it can be shown analytically that there must be at least one value of ω for which the condition for maximum power is satisfied. In the limit as $\omega \to 0$,

$$\mathrm{Im}\{Z_1\} \to \frac{1}{\omega}\left(\boldsymbol{C}_{11} - \frac{\boldsymbol{C}_{01}^2}{\boldsymbol{C}_{00}}\right) = \frac{m_1 g}{\omega l_1}\left(\frac{M_w - M - m_1}{M_w - M - m_1(1 - \delta^2 \hat{l}_1)}\right). \tag{3.50}$$

In order for the device to be buoyant $(M_w - M - m_1)$ must be positive, thus $\mathrm{Im}\{Z_1\}$ tend to positive infinity as $\omega \to 0$. Conversely, as $\omega \to \infty$,

$$\begin{aligned}\mathrm{Im}\{Z_1\} &\to \omega\left(\frac{\boldsymbol{M}_{01}^2}{(\boldsymbol{M}_{00} + A(\infty))} - \boldsymbol{M}_{11}\right) \\ &= -m_1\omega\left(\frac{m_1\hat{k}_1^2 + (1 + \hat{k}_1^2)(M(1 + \delta^2\hat{K}^2) + A(\infty))}{M(1 + \delta^2\hat{K}^2) + m_1\,(1 - \delta\hat{l}_i)^2 + m_1\,(\delta\hat{l}_1\hat{k}_1)^2 + A(\infty)}\right),\end{aligned} \tag{3.51}$$

where $A(\infty) > 0$, implying that $\mathrm{Im}\{Z_1\}$ tends to minus infinity as $\omega \to \infty$. Thus, since $\mathrm{Im}\{Z_1\}$ is a continuous function of ω, there must be at least one value of ω such that $\mathrm{Im}\{Z_1\} = 0$. It will be important that the values of ω for which this is satisfied correspond to a period in the range of interest when considering a typical sea state.

3.6. *Numerical calculations*

To summarize the procedure for calculating the efficiency of the two-dimensional device with N internal pendulums, we use (2.13) with Z defined by (3.22) in terms of A and B, and with λ given by (3.21).

If only one internal pendulum is used, then an alternative calculation of efficiency for the two-dimensional device is given by (3.48) expressed in terms of the elements of the matrix $\boldsymbol{Z}$ in (3.41), the advantage of this system being that the optimum device efficiency over all frequencies is given by (3.49) and that conditions for maximum efficiency are easily tested.

The theory is based on linearized small-amplitude motions. Thus, we have a duty to consider the response of the cylinder and the pendulums as a function of frequency and incident wave amplitude. As before, we are able bypass a direct calculation of X_s by using the Haskind relation (for symmetric bodies)

$$X_s = \tfrac{1}{2}\rho g H A_+ D(kh), \tag{3.52}$$

where H is the incident wave height (peak to trough), A_+ is the far-field radiated wave amplitude to $+\infty$ for the forced surge motion of unit velocity of the cylinder

https://doi.org/10.1017/jfm.2012.557 Published online by Cambridge University Press

introduced previously in the definition of η in § 2.2, $D(kh) = \tanh kh + kh\mathrm{sech}^2 kh$ is a scaling factor in terms of the water depth h and the wavenumber k travelling waves related via the dispersion relation to the frequency by $\omega^2 = gk \tanh kh$.

A second reciprocal relation relates far-field radiated waves to the radiation damping coefficient via

$$B = \rho\omega |A_+|^2 D(kh), \tag{3.53}$$

(see Mei, Stiassnie & Dick 1983, for example). Thus, together (3.52) and (3.53) allow us to eliminate the far-field radiated wave amplitude, A_+, and write an expression for $|X_s|$,

$$|X_s| = \tfrac{1}{2} gH \sqrt{\rho D(kh) B/\omega} \tag{3.54}$$

We recall from the first method (2.6) gave

$$U = \frac{X_s}{Z + \lambda}, \tag{3.55}$$

and combining with (3.54) leads to a cylinder velocity non-dimensionalized by the surface wave velocity,

$$\frac{|U|}{A\omega} = \frac{g\sqrt{\rho DB/\omega}}{\omega |Z + \lambda|} \equiv \frac{g\sqrt{D\nu/\pi}}{\omega^2 a |\hat{Z} + \hat{\lambda}|} \tag{3.56}$$

where $\nu = B/(M_w\omega)$, $\hat{Z} = Z/(M_w\omega)$, $\hat{\lambda} = \lambda/(M_w\omega)$ and $A = H/2$ is the wave amplitude. Note that $|U|/A\omega$ is also the ratio of the amplitude of the cylinder axis excursion to the surface wave amplitude. In terms of the angular displacement of the cylinder, we make the connection $|\Theta| = |U/(L\omega)|$ such that

$$|\Theta/A| = \frac{1}{L}\frac{|U|}{A\omega}, \tag{3.57}$$

as a dimensional measure of the maximum displaced angle of the cylinder per unit amplitude of the incident wave.

Further, the relation (3.17) between u_i and U with $|\theta_i| = |u_i/(l_i\omega)|$ also reveals a similar relation for the maximum excursion, per unit wave amplitude as

$$|\theta_i|/A = \frac{1}{l_i}\left|\frac{1 + \mathrm{i}\hat{\gamma}_i \hat{l}_i \delta}{\hat{\Omega}_i + \mathrm{i}\hat{\gamma}_i}\right| \frac{|U|}{A\omega}, \quad i = 1, \ldots, N \tag{3.58}$$

using (3.56) to substitute for the last factor of the right-hand side.

Following the notation of the second method and with a device containing only one pendulum, writing the equation of motion in matrix form also poses an alternative way of calculating the cylinder and pendulum excursion. Equation (3.40) provides a relation between the velocity vector $\boldsymbol{U}$ and the external hydrodynamic problem, thus we can simply invert and write

$$\boldsymbol{U} = \boldsymbol{E}\boldsymbol{X}_s. \tag{3.59}$$

After using (3.32), (3.26), (3.43) and (3.54) this allows the cylinder and pendulum excursion per unit wave amplitude to be evaluated explicitly, once the connections $|\Theta| = |U/(L\omega)|$ and $|\theta_i| = |u_i/(l_i\omega)|$ have been made.

The only hydrodynamic coefficients that are needed to assess a two-dimensional device are the dimensionless added mass and damping coefficients $\mu = A/M_w$ and

https://doi.org/10.1017/jfm.2012.557 Published online by Cambridge University Press

$\nu = B/(M_w\omega)$ as a function of ω for a submerged circular cylinder in finite depth and these are accessible using well-established multipole methods (see Linton & McIver (2001) or the Appendix of Evans & Porter (2007) for example). Thus, the exciting force X_s is not required in two-dimensional calculations although it is needed for a three-dimensional device (i.e. a finite length cylinder in an unbounded ocean).

Finally, the moment of inertia of the cylinder about its axis has been defined in terms of a radius of gyration K which would probably be close to a for a real device assuming most of the mass of the cylinder is mainly confined to the walls of the cylinder. In all of the computations that follow we have taken $K^2 = 0.8a^2$ although computations are not sensitive to the numerical factor of 0.8.

4. Results for a cylinder with internal pendulums

We concentrate on the two-dimensional version of this device for which simple analytical methods exist for determining the hydrodynamic coefficients $A(\omega)$ and $B(\omega)$ needed for the power calculations.

The first task is to determine the effectiveness of the internal pendulum PTO system. Consequently, it is sensible to compare with the simple pitching cylinder device of § 2 and thus we choose the same parameters, a cylinder of radius $a = 7$ m in water of depth $h = 50$ m, and look for efficiencies close to maximum of $E_{max} = 1/2$ over periods from 5 to 11 s. There is a greater flexibility in the choice of parameters for this new device, including the mooring parameter, δ, and both the number (N) of pendulums and their configuration (ρ_s, b_i, α_i and γ_i). These are in addition to parameters such as the mooring length L, the submergence f and the mass of the cylinder M.

To fix ideas further, let us take $M/M_w = 0.15$ and $a/f = 0.75$ as in § 2 and to simplify initial investigations we consider a single ($N = 1$) pendulum. We assume that the pendulum is made from concrete, $\hat{\rho} = \rho_s/\rho = 2.4$ and this remains unaltered hereafter. Initial numerical investigations reveal that $\hat{b}_1 = b_1/a = 0.5$ and $\alpha_1 = \pi/3$ have the potential to produce promising results. These parameters are fixed throughout the results shown in figure 5 which then predominantly focus on the effect of varying the mooring parameters, δ and L.

In figure 5(*a,c,e*), the imaginary part of $\hat{Z}_1 = Z_1/(M_w\omega)$ is shown as a function of wave period. The purpose of these curves is to mimic the effort made in § 2.3 to determine resonant conditions for the simple pitching cylinder. Here, the situation with a coupled pendulum/cylinder system is more complicated, but we have shown theoretically in § 3 that resonance and the potential for maximum power efficiency correspond to values of frequency when $\mathrm{Im}\{\hat{Z}_1\} = 0$. In figure 5(*b,d,f*) the corresponding plots of E_{opt}, calculated using (3.49) are shown. These are curves which show the optimal efficiency for the system configuration at any given frequency which would be obtained by setting the damping parameter to vary with frequency as $\gamma_1 = |Z_1|$. In figure 5, which have been extended over periods from 3 to 20 s, the correspondence between frequencies at which $\mathrm{Im}\{\hat{Z}_1\} = 0$ and $E_{opt} = 1/2$ can be observed.

In the formulation of the problem it may be noted that mooring parameter, δ, describing the proportional roll with respect to pitch of the cylinder and L, the mooring length, appear in the combination δ/L almost everywhere; the single exception is in the definition of C_N (or $\boldsymbol{C}$) where L is independent from δ. Nevertheless, this suggests that the single dimensionless parameter $\delta a/L$, might be a useful tool for assessing the effect of the two mooring parameters. Thus, in figure 5

https://doi.org/10.1017/jfm.2012.557 Published online by Cambridge University Press

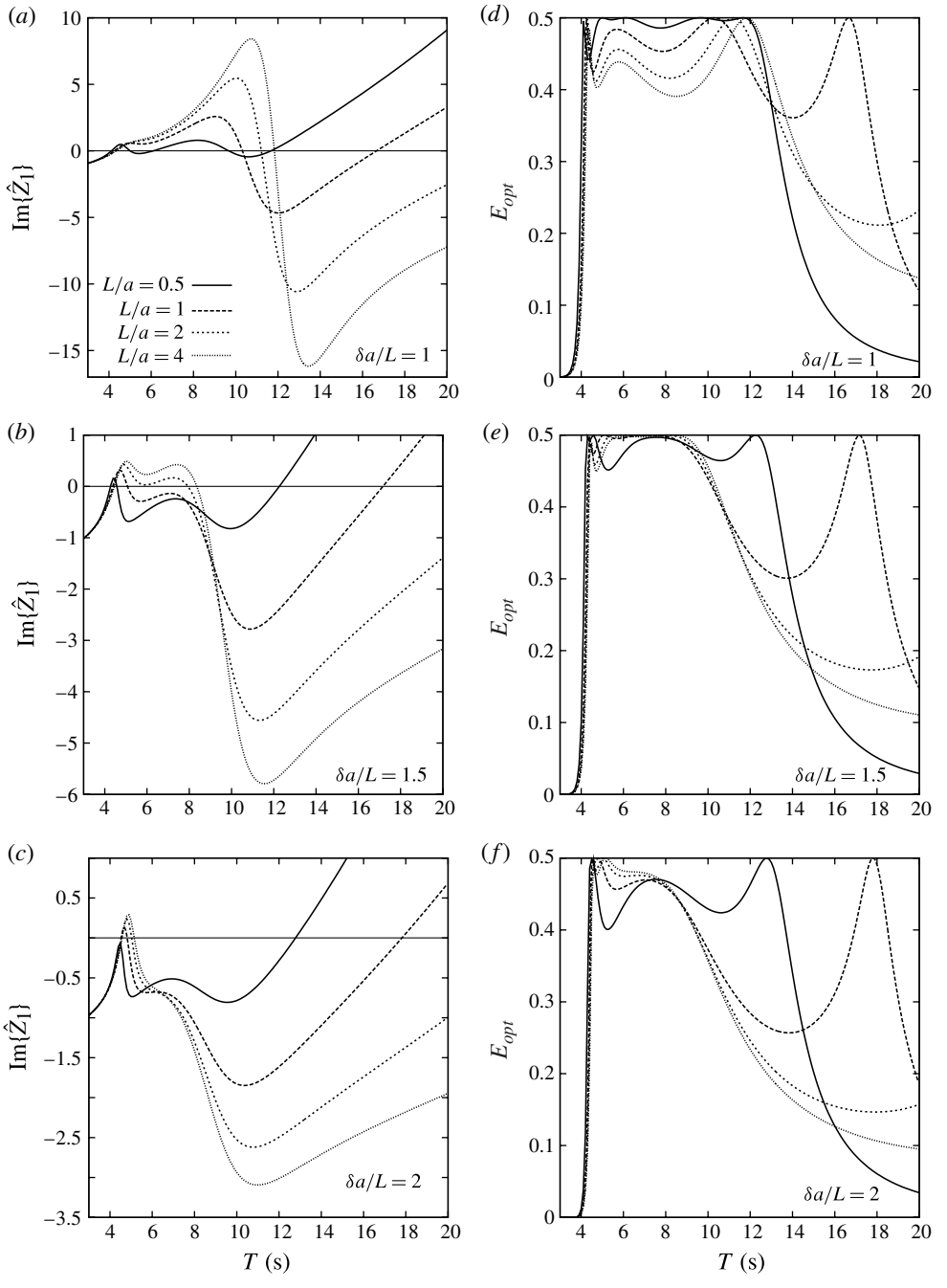


FIGURE 5. For a pitching cylinder device with an internal pendulum: $h = 50$ m, $a = 7$ m, $a/f = 0.75$, $M/M_w = 0.15$, $\hat{\rho} = 2.4$, $\hat{b}_i = 0.5$, $\alpha_i = \pi/3$. In (*a–c*) $\mathrm{Im}\{\hat{Z}_1\}$ is shown for varying values of the roll to pitch length ratio $\delta a/L$. In (*d–f*) the corresponding E_{opt} is shown for the same parameter values.

https://doi.org/10.1017/jfm.2012.557 Published online by Cambridge University Press

we set $\delta a/L = 1$, 1.5 and 2 and within each pair of subfigures let L/a vary with values 0.5, 1, 2 and 4.

One can see for fixed $\delta a/L$ some similarity in the behaviour of the function $\mathrm{Im}\{\hat{Z}_1\}$ as L/a is varied, especially at high frequencies and this is more notable as $\delta a/L$ increases. Also evident from figure 5 is the behaviour of $\mathrm{Im}\{\hat{Z}_1\}$ as $\omega \to 0$ and infinity predicted by (3.50) and (3.51). Within these asymptotic bounds, the function $\mathrm{Im}\{\hat{Z}_1\}$ passes through zero anywhere between just once and five times depending on the parameters chosen. These zeros correspond to resonances and there is a division between those associated with the internal compound pendulum in isolation which is tuned here to 5.2 s and is a persistent feature of figure 5(*a–c*) and those associated with pitching cylinder in isolation which does vary with the mooring system. The coupling between the hydrodynamics, the cylinder and the internal pendulum makes this more complicated than just stated so that, for example, there are no 'internal pendulum resonances' when $L/a = 0.5$ and $\delta a/L = 2$ – see figure 5(*c*). Apart from these peculiarities, another general observation is that a single internal pendulum produces a pair of resonances close to the tuned uncoupled resonance of the pendulum. This is a well-known effect in the small-amplitude oscillations of coupled pendulum systems.

The simplest mooring system from a practical perspective corresponds to $\delta = 1$. Then in figure 5(*a*,*d*) this would correspond to $L/a = 1$ (the long-dashed line). A better response over periods from 5 to 11 s is found in figure 5(*b*,*e*). Now $L/a = 2/3$ and a broad-banded response curve sitting between the solid and the long-dashed lines can be inferred from the figures. In both cases, the pivot is far above the level of the sea bed. If, instead, the cylinder was to be pivoted about a point on the sea bed, then one would require $L/a = 5.81$ under the parameters being considered. Looking at the curves in figure 5, it can be inferred that a good broad-banded response is possible for the largest value of $L/a = 4$ when $\delta a/L = 1.5$ and this would imply a mooring system with $\delta = 6$. Indeed, numerical experiments have allowed us to confirm a general trend that δ must increase roughly in proportion to L/a to retain a broad-banded efficiency. In fact, for the sea bed moored cylinder with $L/a = 5.81$ we have found that the 'optimal' value of δ for this particular system is 8.7. Such large values of δ are unlikely to be adopted in practice and thus we are likely to be confined to considering smaller values of δ and, hence, L/a.

We now investigate one of the configurations presented in figure 5 in more detail: $L/a = 0.5$ and $\delta = 0.5$ which possesses five resonances. The aim is now to select a constant damping coefficient such that the efficiency, E, is both broad-banded and close to E_{max} across our target period range of $T = 5$–11 s.

If $\gamma_1 = \mathrm{Re}\{Z_1\}$ at a resonant frequency, for which $\mathrm{Im}\{Z_1\} = 0$, then $E = E_{max}$ there. Figure 6(*a*) shows the device efficiency when the damping coefficient is tuned to $\gamma_1 = \mathrm{Re}\{Z_1\}$ at $T = T_i^*$ for $i = 1, 3, 5$, three of the five resonant periods. The curve tuned to the period T_3^* happens to give the best efficiency, that is the device response remains closest to 1/2 of those three candidates over the range 5–11 s. However, it is expected that a more broad-banded response could be achieved given a more judicious choice of, or say a numerically selected, damping coefficient. Hence, we choose to numerically minimize the normalized integral of $(\gamma_1 - |Z_1|)^2 / |\gamma_1 + Z_1|^2$ as a function of γ_1 over periods from $T = 5$ to 11 s, thus maximizing the area under the efficiency curve – a process described by Thomas & Gallachóir (1993) for the Bristol Cylinder.

Figure 6(*b*) plots the optimal value of the damping coefficient, i.e. $\tilde{\gamma}_i \equiv \hat{\gamma}_i \sqrt{Ka} = |\hat{Z}_1| \sqrt{Ka}$ that would result in optimum efficiency. The dotted line represents the

https://doi.org/10.1017/jfm.2012.557 Published online by Cambridge University Press

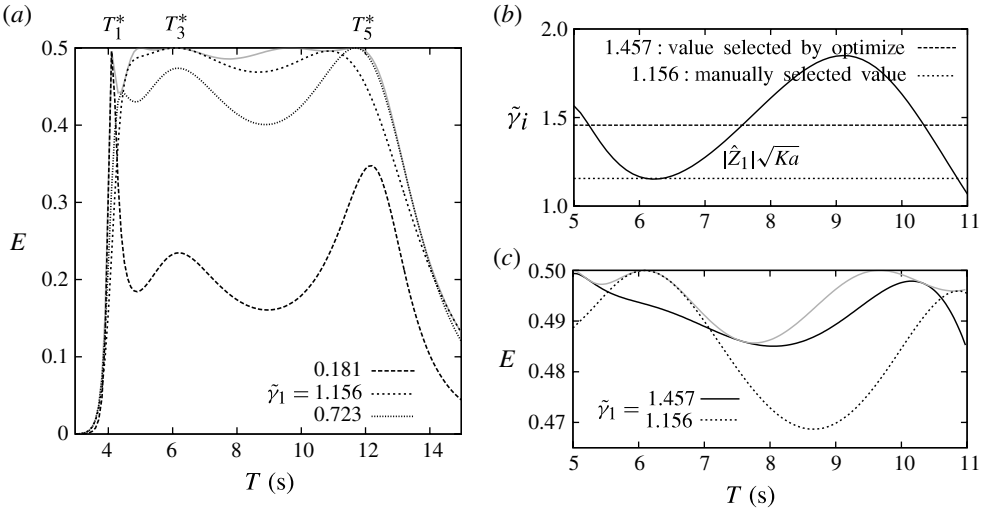


FIGURE 6. A pitching cylinder device with an internal pendulum: $h = 50$ m, $a = 7$ m, $a/f = 0.75$, $s = 0.15$, $\hat{\rho} = 2.4$, $\hat{b}_1 = 0.5$, $\alpha_1 = \pi/3$, $\delta = 0.5$ and $L/a = 0.5$. The points T_i^* indicate three of the five periods for which $\mathrm{Im}\{\hat{Z}_1\} = 0$. In (*a*) E_{opt} is plotted (light grey) along with the efficiency E for different damping coefficients $\tilde{\gamma}_1$. In (*b*) the optimal damping coefficient $\tilde{\gamma}_1 = |\hat{Z}_1|\sqrt{Ka}$ to obtain E_{opt} is shown, along with constant values chosen manually and numerically. In (*c*) the efficiency E for the damping coefficients selected by the optimizer (solid line) and $\hat{\gamma}_1 = \mathrm{Re}\{\hat{Z}_1(T_3^*)\}$ (dotted line) is shown, along with the upper bound E_{opt} (light grey).

value of the damping coefficient chosen to obtain the curve in figure 6(*a*) for $\tilde{\gamma}_1 = |\hat{Z}_1|\sqrt{Ka} = 1.156$ tuned to resonance at $T = T_3^*$ and the dashed line the value chosen by the optimizer.

Figure 6(*c*) plots the efficiency resulting from the use of the optimized damping $\tilde{\gamma}_1 = 1.156$ along with the best manually chosen result from figure 6(*a*), for reference. Although the efficiency of the optimized system fails to reach 1/2 over this range, it does reach E_{opt} three times. Thomas & Gallachóir (1993) refer to this as the detuning effect of the numerical optimizer.

We go on to consider optimized versions of the cylinder devices in three settings. Case A will refer to the large cylinder in deep water ($a = 7$ m, $h = 50$ m) that we have been previously looking at and case B is at half scale ($a = 3.5$ m, $h = 25$ m), both for $\delta = 1$. We also consider case C of a device moored to the sea bed in shallower water ($a = 7$ m, $h = 25$ m, $\delta = 2$, $h = L + f$). With these fixed we extend the previously mentioned numerical minimization routine to optimize the efficiency integrated over the period range 5–11 s in terms of all free parameters, placing bounds on the values where necessary. These include $\alpha_1 \in (0, \pi)$, $\hat{b}_1 \in (0, 1)$, $\hat{\rho} \in (0, 2.4)$, $L/a \in (0, (h - f)/a)$, $a/f \in (0, 0.8)$ and $M/M_w \in (0.15, 0.3)$ in addition to the positive-valued $\tilde{\gamma}_1$. There is a restriction that the total weight of the cylinder plus pendulums does not exceed the weight of water displaced.

Numerical optimization always selects the heaviest pendulums, $\hat{\rho} = 2.4$ and the lightest cylinder $M/M_w = 0.15$. Otherwise the optimal configurations can be quite different depending on the cylinder size and parameters for cases A, B and C are given in table 1.

https://doi.org/10.1017/jfm.2012.557 Published online by Cambridge University Press

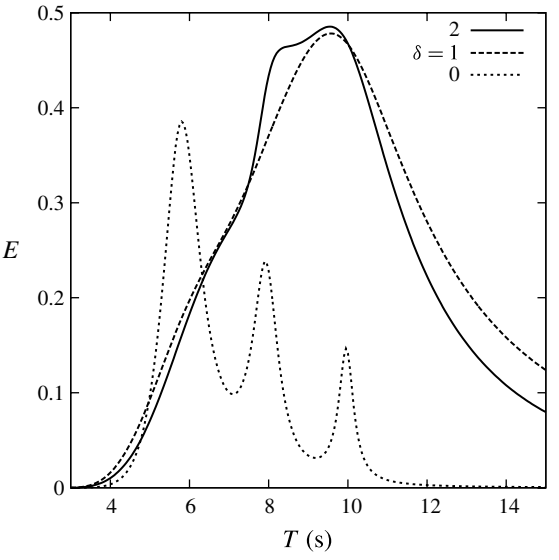


FIGURE 7. Two-dimensional results for a device of radius $a = 7$ m in a sea of depth 50 m with three internal pendulums tuned to 6, 8 and 10 s. Fixing the geometric pendulum configuration, parameters a/f, L/a and $\tilde{\gamma}_i$ for $i = 1, 2, 3$ are optimized over 5–11 s. The device efficiency E is plotted for three different mooring configurations $\delta = 0, 1, 2$.

WEC	Depth (m)	Cylinder radius, a (m)	δ	a/f	L/a	$(M+m_i)/M_w$	$\hat{b}_i$	α_i/π	$\tilde{\gamma}_i$	T_i
A	50	7	1	0.69	0.84	0.58	0.66	0.32	1.05	5.34
B	25	3.5	1	0.80	0.94	0.66	0.59	0.33	1.34	3.74
C	25	7	2	0.54	1.73	0.50	0.57	0.21	2.08	5.00

TABLE 1. Two-dimensional WEC configurations: one pendulum.

We have also considered optimizing over multiple pendulums, $N > 1$, but the numerical optimization appears always to select identical pendulum parameters. An example of a system with three internal pendulums, tuned to fixed wave periods of 6, 8 and 10 s is shown in figure 7. Under a sequence of fixed mooring parameters $\delta = 0$, 1 and 2 and $a = 7$ m, $h = 50$ m and M/M_w the parameters L/a, a/f and damping constants $\tilde{\gamma}_i$, $i = 1, 2, 3$, have been optimized to produce the best efficiency over 5–11 s. One can see only clearly in the case $\delta = 0$ the effect of each pendulum; this is typical that fixing the tuning of the pendulums is not effective. For $\delta = 1$ and 2 is less clear how the system operates, although it is well below the performance of the earlier examples with just one pendulum.

Figure 8(a) shows the efficiency of the two cases A and B against period alongside corresponding optimal curves E_{opt}. It is clear that the device with larger radius (case A) exhibits better performance over the target period range of 5–11 s than the half-scale version. These results are linked to the optimized curves of $\mathrm{Im}\{\hat{Z}_1\}$ in figure 8(b), since $\mathrm{Im}\{\hat{Z}_1\}$ for case A remains closer to zero and for a broader period than case B. Figure 8(c) shows that the angular excursion of both the internal pendulum and

https://doi.org/10.1017/jfm.2012.557 Published online by Cambridge University Press

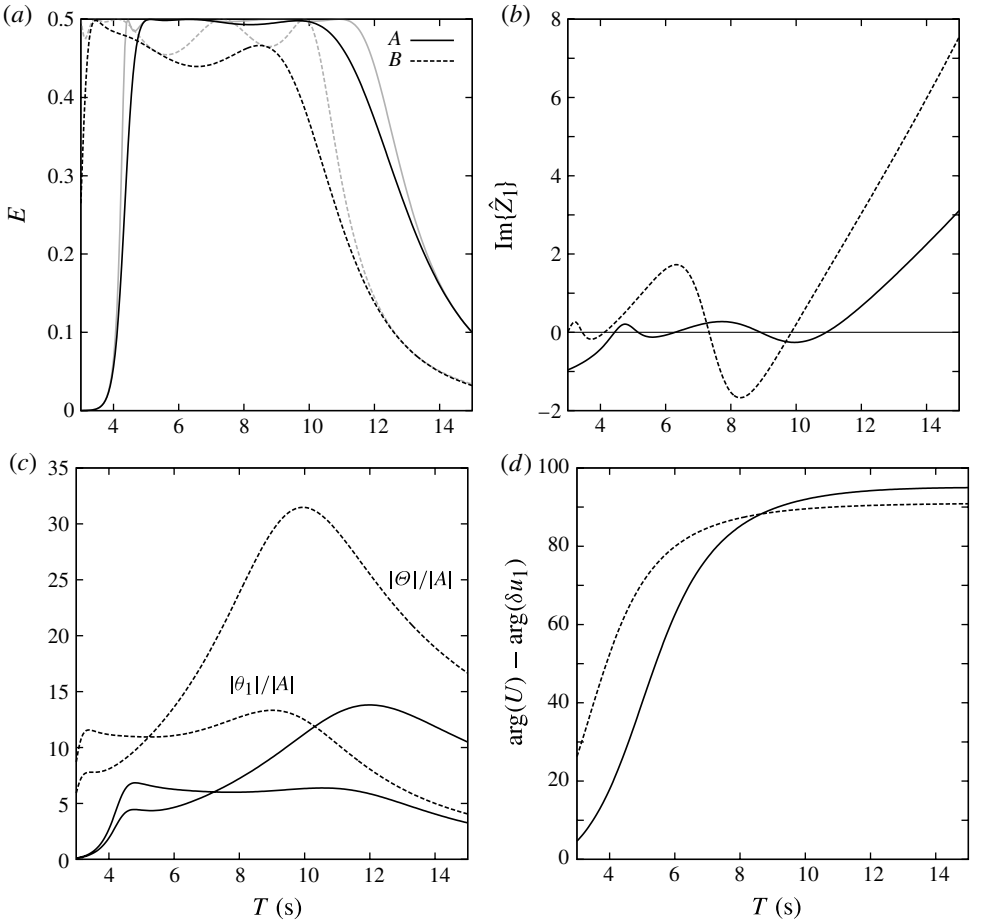


FIGURE 8. Two-dimensional results for two optimized devices A and B, details of which are given in table 1. In (a) the device efficiency E is plotted with its upper bound E_{opt}. In (b) $\mathrm{Im}\{\hat{Z}_1\}$ is shown with $y = 0$ for reference. In (c) the angular pendulum and cylinder excursion is plotted per unit amplitude of incident wave. In (d) the relative phase of the internal pendulum and rolling cylinder is shown.

cylinder, plotted per unit wave amplitude, is small and thus is in line with the small-amplitude motions that were initially assumed. The results indicate that a cylinder of radius 7 m is appropriate for a broad-banded response over 5–11 s and that the half-scale 3.5 m cylinder struggles to be as efficient over the same period range, having to respond with approximately twice the cylinder/pendulum excursion but still able to perform reasonably well. Had the target period range been lower, say 3.5–9 s, then the 3.5 m cylinder could be optimized to perform as well as the 7 m cylinder over 5–11 s.

An example of a cylinder moored directly to the sea bed such that $h = L + f$, case C, is given in figure 9, with $a = 7$ m and $N = 1$ pendulum again but with $h = 25$ m and a $\delta = 2$ mooring. The internal pendulum configuration and a/f are optimized over wave periods 5–11 s and figure 9(a) shows both E_{opt} and the underlying curve E for a fixed optimized damping parameter. In figure 9(b) the associated cylinder and

https://doi.org/10.1017/jfm.2012.557 Published online by Cambridge University Press

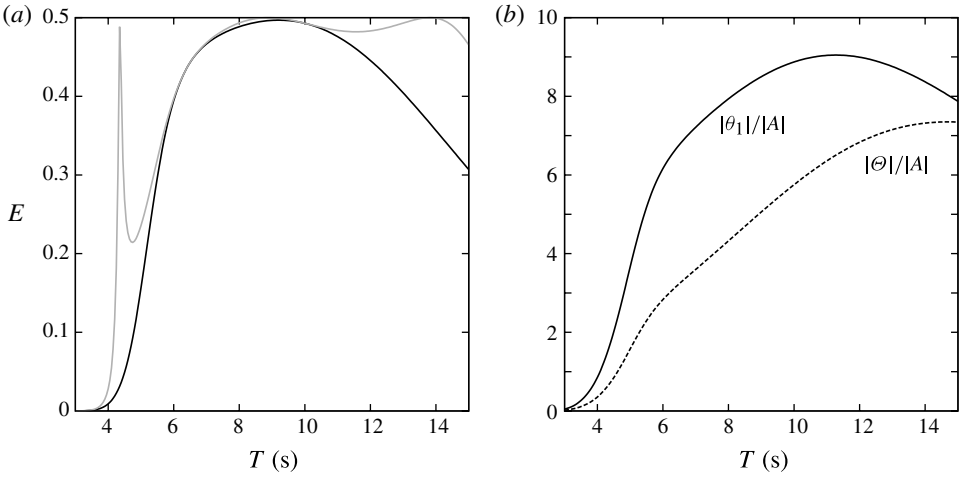


FIGURE 9. Two-dimensional results for an optimized device (C) of radius $a = 7$ m in a sea of depth 25 m, moored such that $\delta = 2$ with pivot points fixed to the sea bed, details of which are given in table 1. In (*a*) the device efficiency E is plotted with its upper bound E_{opt}. In (*b*) the angular pendulum and cylinder excursion is plotted per unit amplitude of incident wave.

pendulum angular excursions are shown per unit incident wave amplitude confirming that linearized theory is an appropriate approximation.

Moored to the sea bed such that $\delta = 2$ the shape of the device response curve for case C is quite different to that of cases A and B. Although the efficiency case C, in figure 9(*a*), decreases to a lesser extent and more slowly at lower frequencies when compared with cases A and B in figure 8(*a*), and despite that efficiencies greater than 40 % are achieved over 6–13 s, the response of case A is far more broad-banded and the efficiency consistently closer to 1/2 over 5–11 s.

4.1. *Three-dimensional theory*

Energy absorption calculations in three dimensions differ only very slightly from their two-dimensional counterparts. Here we will quote modifications to the previously two-dimensional theory for a three-dimensional device consisting of a finite length cylinder in the open sea. In two dimensions, power is measured per unit length of the device and this enables the notion of efficiency to be introduced. In three dimensions, efficiency is replaced by capture width, defined to be the ratio of the mean power taken from the device of length D to the mean power per unit crest length of an incident wave. In other words

$$l = W/W_{inc} \tag{4.1}$$

defines capture width where

$$W_{inc} = \frac{1}{8}\rho g|H|^2 c_g \quad \text{and} \quad c_g = \frac{g}{2\omega}D(kh) \tag{4.2}$$

as before in terms of the wave height H, where c_g is the group velocity and $D(kh) = \tanh kh + kh\mathrm{sech}^2 kh$. Previously derived expressions for power, W, such those as given by (2.11), (2.16) or (3.45), dependent upon the method used, all remain in place but now with A and B now defined as the surge component of the forced surge

https://doi.org/10.1017/jfm.2012.557 Published online by Cambridge University Press

motion for the finite cylinder and with X_s replaced by $X_s(\beta)$, the surge exciting force on the fixed three-dimensional cylinder due to a wave making an angle β with respect to the positive x direction. For example, the maximum mean power a device may absorb is modified by

$$W_{max} = \frac{|X_s(\beta)|^2}{8B}. \tag{4.3}$$

It follows from (4.3) that the maximum capture width is given by

$$l_{max} \equiv \frac{W_{max}}{W_{inc}} = \frac{|X_s(\beta)|^2}{8BW_{inc}}. \tag{4.4}$$

We note that it is purely a function of the geometry of the cylinder; that is, it contains no tunable parameters associated with the internal PTO mechanism nor the mooring system.

It is worth noting that the reciprocal relation (2.12) used in two dimensions to bypass the calculation of X_s in favour of the known quantity $\eta = 1/2$ is replaced in three dimensions by

$$B = \frac{\displaystyle\int_0^{2\pi} |X_s(\theta)|^2 \, \mathrm{d}\theta}{8\Lambda W_{inc}} \tag{4.5}$$

(see Evans 1980, for example), where Λ denotes the incident wavelength. This expression is only simplified for devices with a vertical axis of symmetry. When such a device absorbs in surge, $X_s(\beta) = X_s(0)\cos\beta$ and the well-known result that follows from (4.5) and (4.4) is $l_{max} = \Lambda/\pi$. In our case, there is no vertical axis of symmetry and, hence, the capture width calculation is performed using (4.1) with (4.3) and requires computation of $|X_s(\beta)|$.

A useful alternative to the capture width is the ratio of capture width to device width, often referred to as the capture factor

$$\hat{l} = \frac{l}{D}. \tag{4.6}$$

For a device which is much longer than the incident wavelength, one might expect the device to respond as a two-dimensional cylinder along a large proportion of its length and one might argue that $\hat{l}$ will find it hard to significantly exceed a value of a half, reflecting the fact that the infinitely long cylinder is a maximum of 50 % efficient. For a 'shorter' cylinder, although there is no vertical axis of symmetry, one might expect the values of $\hat{l}$ to feel the influence of the point absorber result of Λ/π.

It is with these arguments in mind that we have computed capture widths as a function of period for two three-dimensional devices in figure 10. Computations for the hydrodynamic coefficients, A and B, and $X_s(\beta)$ have been performed using WAMIT for cylinders of length $D = 28$ and $D = 70$ m, respectively. WAMIT is a commercial boundary element method package based on linear wave theory for analysing the hydrodynamic interaction of three-dimensional floating or submerged bodies of arbitrary geometry with ocean waves. An overview of the use of WAMIT, and other fluid modelling software packages, in problems relating to wave energy conversion is available in Cruz (2008).

In both cases the cylinder is of radius $a = 7$ m in $h = 50$ m water depth with its axis submerged a distance $f = 10$ m below the surface, a configuration which proved to be

https://doi.org/10.1017/jfm.2012.557 Published online by Cambridge University Press

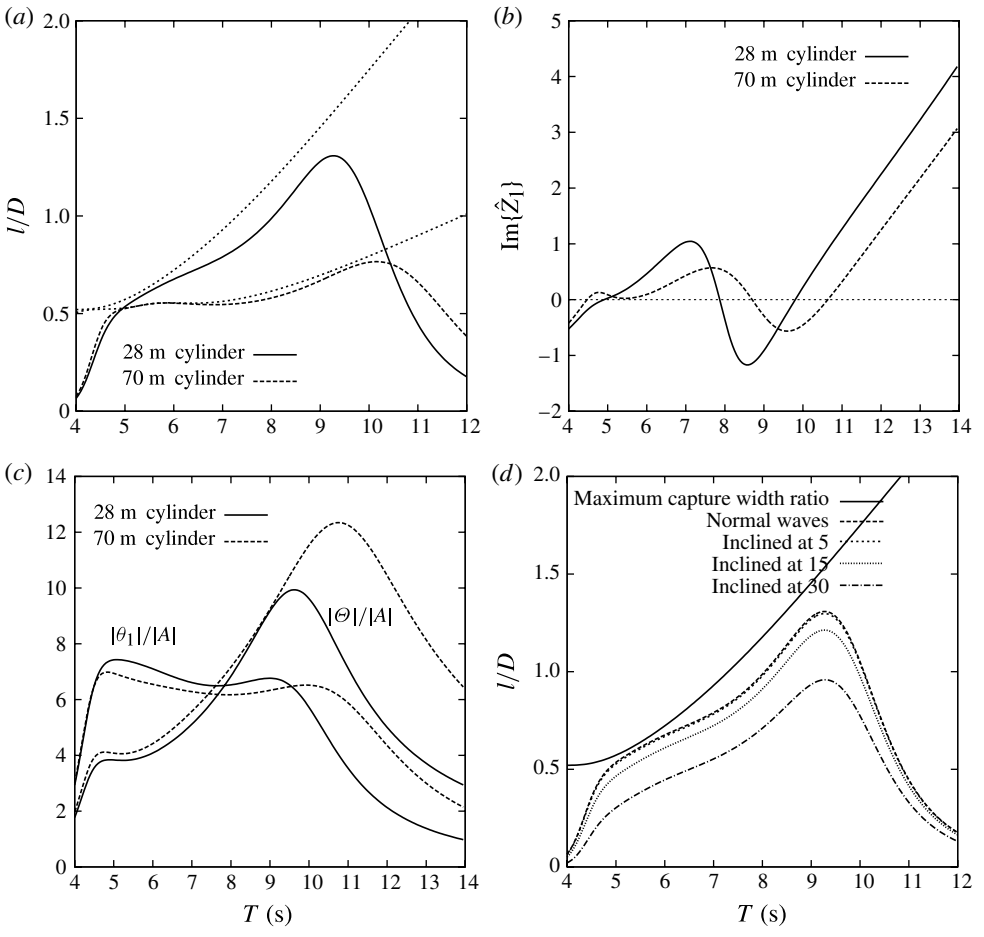


FIGURE 10. Three-dimensional results for two optimized devices of length 28 and 70 m, details of which are given in table 2. In (*a*) the dimensionless capture width per unit length of the device l/D is plotted with its maximum possible value l_{max}/D. In (*b*) $\mathrm{Im}\{\hat{Z}_1\}$ is shown with $y = 0$ for reference. In (*c*) the angular pendulum and cylinder excursion is plotted per unit amplitude of incident wave. In (*d*) the dimensionless capture width per unit length of the device l/D and the maximum possible value l_{max}/D is shown for waves of varying angles of incidence.

optimal in two dimensions (see case *A* in table 1). We fix $\hat{\rho} = 2.4$ and $M/M_w = 0.15$, but allow the dimensions of the pendulums (b_i, α_i) and the damping coefficient $(\tilde{\gamma}_i)$ to be selected by the same numerical optimization procedure working over periods from 5 to 11 s. In each case the device has one pendulum and we have $\delta = 1$ as our mooring system, the numerically optimized parameters are given in table 2.

Thus, figure 10(*a*) which shows both the capture factor and the maximum capture factor for the two cylinder lengths, confirms that the longer cylinder has a capture factor only just above a half, a feature more noticeable for shorter waves. In contrast, the $D = 28$ m cylinder has a much higher capture factor over a large range of periods of interest and takes values in excess of unity between 8 and 10.5 s waves. The shorter cylinder now finds it harder than the longer cylinder to approach the maximum values

https://doi.org/10.1017/jfm.2012.557 Published online by Cambridge University Press

Length, D (m)	L/a	$(M+m_i)/M_w$	$\hat{b}_i$	α_i/π	$\tilde{\gamma}_i$	T_i
28	1.09	0.47	0.78	0.34	0.88	5.55
70	0.93	0.53	0.71	0.31	0.95	5.38

TABLE 2. Three-dimensional WEC configurations, for a cylinder of radius $a = 7$ m in fluid of depth $h = 50$ m with submergence $f = 10$ m.

which have been designed around the two-dimensional optimization. Nevertheless, a broad-banded response persists in this three-dimensional simulation.

In figure 10(*b*) we show the variation of $\mathrm{Im}\{\hat{Z}_1\}$ with period corresponding to the optimized pendulum configurations of figure 10(*a*) for each cylinder length. The curve for the longer cylinder resembles closely that seen in figure 8(*b*) although the shorter cylinder exhibits just three potential resonances. Figure 10(*c*) illustrates that the angular excursion of both the internal pendulum and cylinder for each cylinder length, plotted per unit wave amplitude, remains small enough to find linearized theory appropriate. Again, the results for the longer cylinder are similar to those in figure 8(*c*) although, perhaps surprisingly, the shorter cylinder with the larger capture ratio has generally smaller motions.

Finally, in figure 10(*d*) we illustrate how the capture width of the 28 m device varies for waves of a range of angles of incidence, from normally incident waves to those incident at an angle of 30° to the cylinder. We see that for even for waves inclined at 15°, the WEC still has a capture width ratio greater than a half for waves of period 5.5–11 s.

4.2. *Irregular waves*

In this section we consider the power output of a three-dimensional cylinder device in irregular waves with use of a wave energy spectrum $S(T)$ to represent a more realistic sea state. We employ the two-parameter spectrum developed by Bretschneider (1959),

$$S(T) = \frac{5}{16} H_{1/3}^2 \frac{T^5}{T_p^4} \mathrm{e}^{-5\,(T/T_p)^4\,/4}, \tag{4.7}$$

where $H_{1/3}$ denotes the significant wave height, defined as the mean height of the highest third of waves, and T_p the peak wave period in the spectrum. The average incident wave power per unit crest length is given by

$$\overline{W}_{inc} = \rho g \int_0^\infty c_g(T) S(T) T^{-2}\,\mathrm{d}T, \tag{4.8}$$

in units of kW m^{-1}, where $c_g(T)$ is the group velocity of the waves as a function of period. The depth-dependent group velocity was previously given by (4.2), however since the Bretschneider spectrum was developed for deep water conditions, here we make the same deep water assumption such that $D(kh) = 1$ and $c_g = g/(2\omega)$. Thus, the total mean power absorbed by a device of length D is then

$$\overline{W} = \rho g \int_0^\infty c_g(T) S(T) l(T) T^{-2}\,\mathrm{d}T, \tag{4.9}$$

https://doi.org/10.1017/jfm.2012.557 Published online by Cambridge University Press

	0°	5°	15°	30°
$\overline{W}$ (kW)	740	733	682	530
$\bar{l}$	0.894	0.886	0.824	0.640

TABLE 3. Total mean power absorbed by the device.

where $l(T)$ is the capture width of the device given by (4.1) expressed here as a function of period, T. As before we can define a dimensionless mean capture factor,

$$\bar{l} = \frac{\overline{W}}{\overline{W}_{inc} D}, \tag{4.10}$$

which describes the mean proportion of incident wave power absorbed per unit length of the device. This now allows us to simply optimize the total mean power absorbed by the device as opposed to the capture efficiency which does not take into account the varying spectral wave energy density across wave period.

We take typical values of wave height and peak wave period with $H = 2$ m, such that $H_s = 2.83$ m and $T_p = 9$ s which represents a model sea state with an annual average power of approximately 30 kW m^{-1} (see Falnes 2007, for example).

Table 3 gives the power output and dimensionless mean capture factor of the 28 m device introduced earlier for waves of varying angles of incidence. The pendulum configuration is determined by an optimization routine that is only concerned with maximizing the total mean power absorbed by the device in normally incident waves. For the model sea state given above, the 28 m device is predicted to output 740 kW, assuming no losses. This translates to an average absorption of 26.4 kW m^{-1} of the device, not far below the 30 kW m^{-1} incident on it. In other words, the device has a 'mean capture factor' of close to one. As for the two-dimensional device, the output remains of a similar order of magnitude for waves inclined up to 15° on the device. A more sophisticated sea state with built in directional spreading could also have been used.

5. Conclusions

A new concept for the conversion of ocean wave energy into useful energy has been considered in this paper. The WEC comprises a tethered submerged buoyant cylinder containing an internal mechanical system of compound pendulums whose rotation relative to that of the cylinder provides the power. The first part of the paper demonstrates the most important feature of the idea presented, namely that a buoyant cylinder allowed to pitch about a point below the cylinder axis can exhibit multiple resonances over a range of wave periods of interest. The inclusion of a system of N internal pendulums each capable of being tuned to its own period promises to enhance the potential for multiple resonances. However, a series of numerical experiments, some features of which have been illustrated in this paper, and the use of numerical optimization methods have shown that the optimal configuration in nearly all cases is for there to be just $N = 1$ internal pendulum taking off the power. This result reinforces the view that the cylinder is the important component in the system and that the purpose of the single internal pendulum is to provide a frame of reference about which the rotation of the pitching cylinder can extract power.

https://doi.org/10.1017/jfm.2012.557 Published online by Cambridge University Press

The theoretical concept presented is not as sophisticated as the original Bristol cylinder device, but it incorporates features which we believe make the idea attractive to engineers. These include using the mooring as a passive component in the PTO mechanism, incorporating the PTO system internally to the main device and avoiding problems with 'end stops'. Despite being only 50 % efficient in two dimensions, the multiple resonances exhibited by the device being proposed allow it to be close to 50 % efficient over a broad range of wave frequencies. Furthermore, in three dimensions, the device is shown to operate much better than the two-dimensional results would suggest, with a particular (unoptimized) arrangement having a mean capture factor for an irregular sea spectrum of close to one.

Mathematically, two approaches to formulating calculations of wave power have been developed. The challenge here has been to present and arrange equations for motion in $N + 1$ degrees of freedom into informative and practical calculations of power when N of the modes of motion are being damped independently. Each method has particular attributes which have been highlighted within the paper.

The availability of numerically efficient methods for calculating hydrodynamic coefficients in two dimensions has meant that much of the focus has been on demonstrating the optimization of the device parameters in a two-dimensional setting. However, the provision of two sets of numerical data for cylinders of finite length have allowed us to demonstrate a limited optimization in three dimensions, and subject to a model sea state. Further optimization of the cylinder geometry (length, radius, submergence) is now required to increase the power absorption capacity of the device.

The need for large internal masses acting as the pendulums inside the cylinder is one particular concern for this concept. A future development of the idea presented here will be to replace the internal pendulums with water, the sloshing of which will be used to drive air turbines to generate power.

Acknowledgement

The authors would like to thank Dr M. Folley at Queens University, Belfast for providing numerical data for the calculations of power from a finite length cylinder.

REFERENCES

BABARIT, A., CLEMENT, A. H., RUER, J. & TARTIVEL, C. 2006 SEAREV: a fully integrated wave energy converter. In *Proceedings of the OWEMES*.

BRETSCHNEIDER, C. L. 1959 Wave variability and wave spectra for wind-generated gravity waves, U.S. Army Corps of Engineers, Beach Erosion Board, 118.

CHAPLIN, R. V. & AGGIDIS, G. A. 2007 An investigation into power from pitch–surge point-absorber wave energy converters. In *International Conference on Clean Electrical Power*, pp. 520–525. IEEE.

CLARE, R., EVANS, D. V. & SHAW, T. L. 1982 Harnessing sea wave energy by a submerged cylinder device. *ICE Proceedings* **73**, 565–585.

CRUZ, J. 2008 Ocean wave energy: current status and future perspectives. *Green Energy and Technology*, Springer.

EVANS, D. V. 1976 A theory for wave-power absorption by oscillating bodies. *J. Fluid Mech.* **77** (1), 1–25.

EVANS, D. V. 1980 Some analytic results for two and three-dimensional wave-energy absorbers. *Power Sea Waves* 213–249.

EVANS, D. V. 1981 Power from water waves. *Annu. Rev. Fluid Mech.* **13** (1), 157–187.

EVANS, D. V., JEFFREY, D. C., SALTER, S. H. & TAYLOR, J. R. M. 1979 Submerged cylinder wave energy device: theory and experiment. *Appl. Ocean Res.* **1** (1), 3–12.

https://doi.org/10.1017/jfm.2012.557 Published online by Cambridge University Press

EVANS, D. V. & PORTER, R. 2007 Wave-free motions of isolated bodies and the existence of motion trapped modes. *J. Fluid Mech.* **584**, 225–234.

EVANS, D. V. & PORTER, R. 2012 Wave energy extraction by coupled resonant absorbers. *Phil. Trans. R. Soc.* A **370** (1959), 315–344.

FALCÃO, A. F. O. 2010 Wave energy utilization: a review of the technologies. *Renew. Sustainable Energy Rev.* **14** (3), 899–918.

FALNES, J. 2002 *Ocean Waves and Oscillating Systems: Linear Interactions Including Wave-energy Extraction*. Cambridge University Press.

FALNES, J. 2007 A review of wave-energy extraction. *Mar. Struct.* **20** (4), 185–201.

FOLLEY, M., WHITTAKER, T. & VANT HOFF, J. 2007 The design of small sea bed-mounted bottom-hinged wave energy converters. In *Proceedings of the 5th European Wave and Tidal Energy Conference, Porto, Portugal*.

GOLDSTEIN, H. 1974 *Classical Mechanics*. Addison-Wesley.

KASHIWAGI, K., NISHIMATSU, S. & SAKAI, K. 2012 Wave-energy absorption efficiency by a rotating pendulum-type electric-power generator installed inside a floating body. In *Proceedings of the 27th International Workshop on Water Waves and Floating Bodies, Copenhagen, Denmark*.

KORDE, U. A. 1990 Study of a wave energy device for possible application in communication and spacecraft propulsion. *Ocean Engng* **17** (6), 587–599.

LINTON, C. M. & MCIVER, P. 2001 *Handbook of Mathematical Techniques for Wave/Structure Interactions*. Chapman and Hall CRC.

MEI, C. C. 1976 Power extraction from water waves. *J. Ship Res.* **20**, 63–66.

MEI, C. C., STIASSNIE, M. & DICK, K. P. Y. 1983 *Theory and Applications of Ocean Surface Waves*. World Scientific.

NEWMAN, J. N. 1976 The interaction of stationary vessels with regular waves. In *Proceedings 11th Symposium on Naval Hydrodynamics*, pp. 491–501.

NEWMAN, J. N. & LEE, C. H. 2012 WAMIT user manual. http://www.wamit.com.

PARKS, P. C. 1980 Wedges, plates and waves – some simple mathematical models of wave power machines. In *Power from Sea Waves* (ed. B. Count). pp. 257–263. Academic.

SALTER, S. H. 1974 Wave power. *Nature* **249** (5459), 720–724.

SALTER, S. H. 1982 The use of gyros as a reference frame in wave energy converters. In *The 2nd International Symposium on Wave Energy Utilization*.

THOMAS, G. P. & GALLACHÓIR, B. P. 1993 An assessment of design parameters for the bristol cylinder. In *Proceedings of the First European Wave Energy Symposium, Edinburgh, Scotland*, pp. 139–144.

https://doi.org/10.1017/jfm.2012.557 Published online by Cambridge University Press